Therapeutic Helminth Infection of Macaques with Idiopathic Chronic Diarrhea Alters the Inflammatory Signature and Mucosal Microbiota of the Colon

Mara Jana Broadhurst[1]*, Amir Ardeshir[2], Bittoo Kanwar[1], Julie Mirpuri[3], Uma Mahesh Gundra[4], Jacqueline M. Leung[4], Kirsten E. Wiens[4], Ivan Vujkovic-Cvijin[1], Charlie C. Kim[1], Felix Yarovinsky[3], Nicholas W. Lerche[2†], Joseph M. McCune[1], P'ng Loke[4]*

1 Division of Experimental Medicine, Department of Medicine, University of California San Francisco, San Francisco, California, United States of America, **2** California National Primate Research Center, Davis, California, United States of America, **3** Department of Immunology, University of Texas Southwestern Medical Center, Dallas, Texas, United States of America, **4** Department of Microbiology, New York University, New York, New York, United States of America

Abstract

Idiopathic chronic diarrhea (ICD) is a leading cause of morbidity amongst rhesus monkeys kept in captivity. Here, we show that exposure of affected animals to the whipworm *Trichuris trichiura* led to clinical improvement in fecal consistency, accompanied by weight gain, in four out of the five treated monkeys. By flow cytometry analysis of pinch biopsies collected during colonoscopies before and after treatment, we found an induction of a mucosal T_H2 response following helminth treatment that was associated with a decrease in activated $CD4^+$ Ki67+ cells. In parallel, expression profiling with oligonucleotide microarrays and real-time PCR analysis revealed reductions in T_H1-type inflammatory gene expression and increased expression of genes associated with IgE signaling, mast cell activation, eosinophil recruitment, alternative activation of macrophages, and worm expulsion. By quantifying bacterial 16S rRNA in pinch biopsies using real-time PCR analysis, we found reduced bacterial attachment to the intestinal mucosa post-treatment. Finally, deep sequencing of bacterial 16S rRNA revealed changes to the composition of microbial communities attached to the intestinal mucosa following helminth treatment. Thus, the genus *Streptophyta* of the phylum Cyanobacteria was vastly increased in abundance in three out of five ICD monkeys relative to healthy controls, but was reduced to control levels post-treatment; by contrast, the phylum Tenericutes was expanded post-treatment. These findings suggest that helminth treatment in primates can ameliorate colitis by restoring mucosal barrier functions and reducing overall bacterial attachment, and also by altering the communities of attached bacteria. These results also define ICD in monkeys as a tractable preclinical model for ulcerative colitis in which these effects can be further investigated.

Citation: Broadhurst MJ, Ardeshir A, Kanwar B, Mirpuri J, Gundra UM, et al. (2012) Therapeutic Helminth Infection of Macaques with Idiopathic Chronic Diarrhea Alters the Inflammatory Signature and Mucosal Microbiota of the Colon. PLoS Pathog 8(11): e1003000. doi:10.1371/journal.ppat.1003000

Editor: Daniel C. Douek, National Institutes of Health, National Institute of Allergy and Infectious Diseases, United States of America

Received June 27, 2012; **Accepted** September 13, 2012; **Published** November 15, 2012

Copyright: © 2012 Broadhurst et al. This is an open-access article distributed under the terms of the Creative Commons Attribution License, which permits unrestricted use, distribution, and reproduction in any medium, provided the original author and source are credited.

Funding: This work was supported by grants to P.L. and J.M.M. from the California National Primate Research Center (5P51RR000169-48 Loke) and the National Institutes of Health, including a National Institutes of Health Director's Pioneer Award (DPI OD00329) to J.M.M. and startup funds from NYU medical center to P.L. The funders had no role in study design, data collection and analysis, decision to publish, or preparation of the manuscript.

Competing Interests: The authors have declared that no competing interests exist.

* E-mail: mara.broadhurst@ucsf.edu (MJB); Png.loke@nyumc.org (PL)

† Deceased.

Introduction

The incidence of inflammatory bowel diseases (IBD) is highest in industrialized regions wherein helminth infections have been largely eliminated, raising the hypothesis that helminths may protect against intestinal inflammation underlying the disease [1]. Indeed, there is evidence that experimental helminth treatment can ameliorate symptoms in IBD patients [2,3] and in mice [4,5,6,7]. This effect may be attributable to the induction of immunoregulatory networks [8,9] and mucosal repair by a T_H2-type immune response [10,11]. The pig whipworm, *T. suis*, is currently being used in clinical trials to alleviate symptoms in IBD patients, but the mucosal immune responses in treated patients has not been investigated [11].

Recently, we characterized the mucosal responses of an ulcerative colitis (UC) patient who self-infected with the human parasite *T. trichiura* [12]. These studies led to the proposal that the T_H2 immune response activated for parasite clearance, as well as the induction of IL-22 expression, may promote mucosal healing in UC patients by increasing mucus production and turnover of intestinal epithelial cells [11]. In a different study, the mucosal responses of celiac disease patients were examined in detail after experimental treatment with human hookworm infection, showing a suppression of T_H17 responses and upregulation of IL-22 [13,14,15]. This growing body of clinical evidence suggests that a better understanding of mucosal responses activated by helminth infections may contribute to new IBD therapies. Non-rodent, preclinical models of IBD are lacking, and would greatly benefit the development of such novel therapeutics.

ICD, leading to progressive weight loss and dehydration [16], frequently afflicts captive juvenile rhesus macaques (*Macaca mulatta*) and is a leading cause of death at primate research centers. The clinical management of these animals is difficult because the

Author Summary

Young macaques kept in captivity at Primate Research Centers often develop chronic diarrhea, which is difficult to treat because it is poorly understood. This disease shares many features with ulcerative colitis, which is an autoimmune disease affecting the intestinal tract of humans. Recently, parasitic worms have been used in clinical trials to treat inflammatory bowel diseases in humans with positive results, but very little is known about how worms can improve symptoms. We performed a trial where we treated macaques suffering from chronic diarrhea with human whipworms, collecting gut biopsies before and after treatment. We found that 4 out of the 5 treated macaques improved their symptoms and studied the changes in their gut immune responses, as they got better. We found that after treatment with worms, the monkeys had less bacteria attached to their intestinal wall and a reduced inflammatory response to the gut bacteria. Additionally, the composition of gut bacteria was altered in the sick macaques and was restored close to normal after treatment with whipworms. These results provide a potential mechanism by which parasitic worms may improve the symptoms of intestinal inflammation, by reducing the immune response against intestinal bacteria.

condition is often refractory to available treatment. Intestinal inflammatory pathology during ICD can be similar to that found in UC and it has been suggested that ICD may be an informative model for UC [17,18]. As in the case of UC, inflammation is more severe in the colon than in the jejunum and it has been shown that dysregulation of IL-6-STAT3 activation may be an important inflammatory mediator [19]. In this study, we sought to characterize the mucosal inflammatory response driving ICD in the rhesus monkey, and to determine whether helminth exposure can modulate this inflammatory response and lead to clinical improvement.

It is conceivable that the protective effects of helminth treatment for IBD patients may be partly attributable to alterations in the microbial communities of the intestinal tract [11,20]. Changes to the intestinal mucosa by helminth infection [21] are likely to have a major impact on the gut microbial environment [11]. *H. polygyrus* infection has been shown to have major effects on the microbiota of mice, especially increasing the abundance of the Lactobacillaceae family [20]. Colonization of the colon with *T. muris* has been shown to be dependent on the gut microbiota [22]. Uncultured bacterial communities can now be analyzed using DNA barcoding and deep sequencing approaches to investigate how interactions between communities can influence disease pathogenesis [23,24]. In a previous cross-sectional study, McKenna *et al.* investigated the microbiome of healthy macaques in comparison to macaques with chronic diarrhea and after SIV infection [25], finding that bacterial diversity was significantly lower and the family Campylobacteraceae was more common in monkeys with colitis. In this study, we have measured the quantity of attached bacteria to the intestinal mucosa pre-and post-helminth treatment, and further characterized the composition of bacterial communities by deep sequencing in order to determine whether helminth treatment alters the communities of attached bacteria within the intestinal tract of macaques with ICD.

Results

Clinical responses to *T. trichiura* ova

Five juvenile rhesus macaques diagnosed with ICD were enrolled (see Methods for selection criteria) and monitored daily before and after oral administration of 1000 *T. trichiura* ova (Figure 1). The extent of diarrhea (Figure 1) was scored daily and an improvement in fecal consistency (Figure 1A), accompanied by weight gain (Figure 1B), was observed in four out of the five monkeys (TC01–TC04) following *T. trichiura* treatment. Subject TC05 continued to have severe diarrhea and weight loss, and eventually had to be euthanized. Importantly, patent infection was not established in any of the monkeys despite symptomatic improvements and eggs were never detected in the feces. Spontaneous remission does not typically occur in untreated animals, which maintain similar fecal consistency scores in other experiments (Figure S1).

Flow cytometry analyses of leukocytes from pinch biopsies show increased mucosal T_H2 responses and reduced immune activation

To assess changes to the intestinal mucosa before and after helminth treatment, colonoscopies were performed and mucosal biopsies were collected from the five animals prior to treatment, as well as from two healthy, age-matched controls. A second colonoscopy was performed on the ICD subjects 14 weeks after oral administration of *T. trichiura* ova. Peripheral blood mononuclear cells (PBMC) and lamina propria mononuclear cells (LPMC) harvested from colon biopsies were stimulated with PMA and ionomycin for intracellular cytokine staining and flow cytometry analysis (FACS). The proportion of colonic $CD4^+$ T cells producing IL-4, but not those producing IFNγ, was significantly higher ($p<0.001$) following *T. trichiura* treatment (Figure 2A), revealing a localized T_H2 response. In PBMCs, we did not detect more $CD4^+$ T cells producing IL-4 after treatment (data not shown). All five ICD subjects demonstrated this response, indicating that the lack of clinical improvement in subject TC05 was not due to the absence of a T_H2 response. The colonic mucosa of ICD subjects also showed a higher proportion of $Ki67^+$ $CD4^+$ T cells (Figure 2B), indicative of ongoing inflammation. The four clinical responders showed a diminished fraction of such cells following *T. trichiura* treatment, while their proportion actually increased in subject TC05. The proportion of $FoxP3^+$ $CD4^+$ regulatory T (T_{reg}) cells was greater in the colonic mucosa of the ICD subjects compared to healthy controls and was markedly reduced in three out of four clinical responders following *T. trichiura* treatment (Figure 2C). This observation suggests that the local expansion of T_{regs} in these subjects was reflective of active ongoing inflammation.

Transcriptional profiling analysis demonstrates alterations to inflammatory gene expression patterns in response to *T. trichiura* treatment

We isolated RNA from pinch biopsies paired with the samples used for FACS analysis. Whole genome expression profiling of colon biopsy samples identified 185 transcripts that distinguished the inflamed mucosa of ICD subjects (prior to *T. trichiura* treatment) from healthy colon tissue (Figure 3A, Figure S2, Table S1). The genes upregulated in ICD samples included classical T_H1-type inflammatory mediators such as inducible nitic oxide synthase (NOS2), chemokines (CXCL9, CXCL10, CXCL11), and serum amyloid A (SAA1, SAA3, SAA4). IBD-associated genes implicated in mucosal injury and defense [including regenerative factors (REG1, REG3), trefoil peptides (TFF1), and defensins (MNP2, ROAD1, ROAD2)] were also upregulated in ICD samples. This transcriptional signature is consistent with previous studies on UC patients [12,26] and could be driven by attached mucosal microbiota [26]. Pathway analysis indicates enrichment

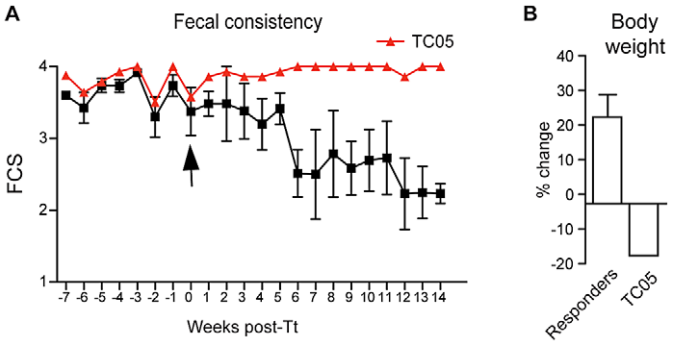

Figure 1. Clinical improvement of juvenile macaques with chronic diarrhea following *T. trichiura* treatment. (**A**) Diarrhea of five macaques was scored daily before and after oral administration of germinated *T. trichiura* (Tt) ova. Fecal consistency scores (FCS) were based on a standardized 4-point scale; 1 = Well-formed, normal; 1.5 = Normal to semi-solid; 2 = Semi-solid to normal; 2.5 = Semi-solid; 3 = Semi-solid to liquid; 3.5 = Liquid to semi-solid; 4 = Liquid. Semi solid stool is defined as "porridge-like" or able to be picked up with a fork. Each score represents the average of daily scores per week. Subject TC05 (red line) showed no clinical response while four other responder animals (TR01-TR04; black line) had a decrease in FCS. (**B**) Change in body weight at 14 weeks following *T. trichiura* treatment, expressed as a percentage of body weight at the time of egg administration. Tt refers to *T. trichiura* treatment.
doi:10.1371/journal.ppat.1003000.g001

for genes in the biological processes that include the JNK cascade, MAPKKK cascade, response to IFN-g, IκB Kinase/NF-κb cascade and macrophage activation as shown in Figure 3B.

Changes in gene expression induced by helminth treatment were also evaluated and 99 transcripts were found to be significantly altered following *T. trichiura* treatment (Figure 3B, Figure S3, Table S2). Notably, many of the IBD-associated genes identified in ICD samples were downregulated following *T. trichiura* treatment. Furthermore, post-treatment samples demonstrated the induction of T_H2-type immune response pathways, including those associated with IgE signaling (FCER1A, MS4A2), mast cell activation (CPA3, CMA1), T_H2 and eosinophil recruitment (CCL17, CCL18, CCL26), alternative activation of macrophages (ALOX5, ALOX15), cytokine signaling (IL5RA, IL9R, POSTN), and worm expulsion (RELMB). This shift was confirmed by quantitative reverse transcription (qRT)-PCR (Figure 4). KEGG pathway analysis showed significant ($P = 0.0136$) enrichment for genes in the arachidonic acid pathway (ALOX5, ALOX15, LTC4S, PTGS1) indicating the production of prostaglandins, which are important regulators of the inflammatory response [27].

The transcriptional profile of subject TC05 clustered separately from the four clinical responders, a distinction primarily driven by a group of immunoglobulin-related transcripts present at much lower levels in this subject (Figure S4 and Table S3). TC05 did not demonstrate a shift from a T_H1-type to T_H2-type gene expression pattern following *T. trichiura* treatment as seen in the four responders, resulting in the close hierarchical clustering between pre- and post-treatment samples from this animal. This observation was confirmed by qRT-PCR (Figure 4), as TC05 did not show reduced expression of certain type-1 inflammatory genes (NOS2, IL1A) or increased expression of T_H2-type response genes (CCL18, CALPAIN13, RELMB) following *T. trichiura* treatment.

Increased bacterial attachment to the intestinal mucosa during ICD

Since IBD may be driven by an aberrant immune response against commensal gut bacteria due to changes in bacterial attachment to the intestinal mucosa [28,29], we quantified the abundance of several bacterial taxa in colon biopsy samples using quantitative PCR for 16S ribosomal RNA genes. Biopsies from each ICD subject demonstrated a higher abundance of multiple taxa compared to healthy controls, revealing a broad increase in bacterial attachment (Figure 5A). Bacterial attachment was reduced following *T. trichiura* treatment, suggesting that the defective mucosal barrier was partially restored. Surprisingly, the bacterial loads in biopsies from TC05 were only slightly higher than those found in control biopsies and only slightly reduced post treatment, suggesting that increased bacterial attachment may not have driven colitis in this subject. One possibility would be that subject TC05 is more sensitive to bacterial translocation even with small quantities of attached bacteria because of an inherently leaky mucosal barrier. Consistent with this possibility, only TC05 showed an increase in serum soluble CD14 (a correlate of microbial product translocation across the mucosal barrier [30]) following *T. trichiura* treatment (Figure 5B).

Changes to the composition of attached bacteria in response to *T. trichiura* ova

In addition to an increased bacterial load, changes to bacterial taxa may be linked with disease pathogenesis. To investigate the composition of microbial communities attached to the intestinal mucosa through culture-independent methods, deep sequencing analysis was performed on the variable region 4 (V4) region of bacterial 16S rRNA [31]. On average, 8439 ± 1373 (SD) sequences were obtained per sample. The microbial diversity within each sample (α-diversity) was compared between biopsies taken from control macaques and from macaques pre-treatment and post-treatment by measuring the Shannon index and phylogenetic diversity (PD) through rarefaction curves (Figure 6A and S5). Shannon diversity was higher in samples post-treatment compared to pre-treatment samples [although not statistically significant ($P = 0.0752$)] and similar to control samples, suggesting that helminth treatment promoted the restoration of the diversity of mucosal microbial communities.

We then performed a Principal Coordinates Analysis (PCoA) on the unweighted UniFrac distances between samples to analyze differences between microbial communities (β-diversity). We observed clustering of control samples with post-treatment samples and the separation of these samples with pre-treatment samples along the PC2 axis (Figure 6C). Clustering patterns generated with Unweighted Pair Group Method with Arithmetic mean (UPGMA) trees were consistent with the PCoA plot (Figure S5). Interestingly, the non-responder TC05 was found to cluster separately from the

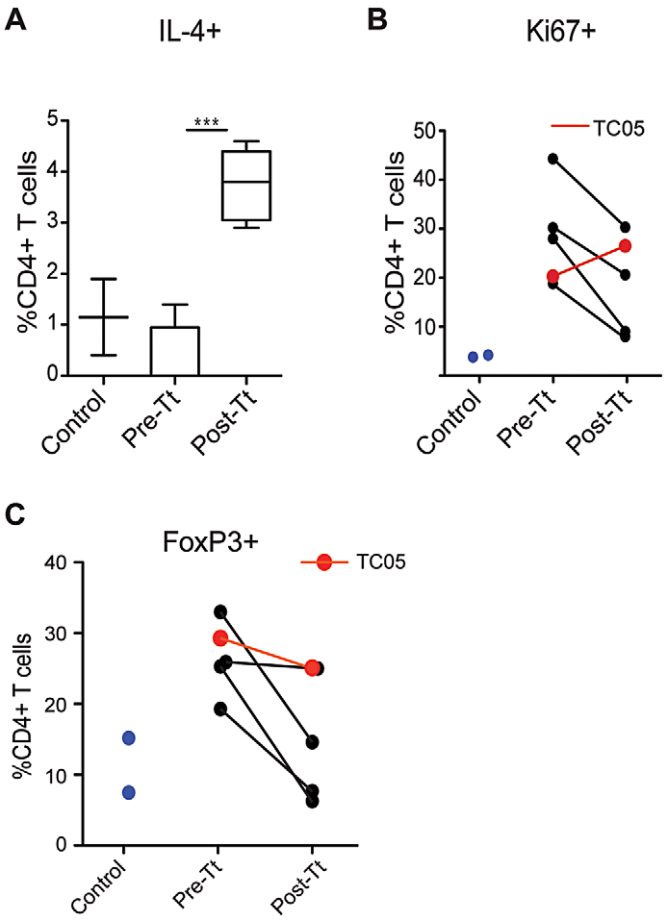

Figure 2. Flow cytometric analysis of CD4$^+$ T cells from colon biopsies following *T. trichiura* treatment. Pinch biopsies collected during colonoscopies pre-treatment (Pre-Tt) and 14 weeks post-treatment (Post-Tt) were compared with samples collected from healthy age-matched controls (Control). Lamina propria mononuclear cells (LPMCs) from biopsies were stimulated *ex vivo* with PMA and ionomycin for intracellular cytokine staining. (**A**) Box and whisker plot showing the percentage of IL-4+ cells among CD4+ LPMCs. ***$p<0.001$, determined by Student's *t*-test. LPMCs were also stained *ex vivo* for intranuclear (**B**) Ki67 and (**C**) FoxP3. Lines connect paired samples from the same subjects pre- and post-treatment. The non-responding macaque (TC05) is shown in red.
doi:10.1371/journal.ppat.1003000.g002

other macaques both pre- and post-treatment. By overlaying taxonomic information onto the PCoA plot, we could illustrate that the phyla Bacteroidetes, Firmicutes, and Tenericutes contribute towards the clustering of control and post-treatment samples, whereas Cyanobacteria contributes towards the clustering of the pre-treatment samples (Figure 6C). Indeed, it was striking to find that in three out of the five macaques pre-treatment samples, the bacterial phylum Cyanobacteria was vastly increased in abundance, representing between 10.8–32.9% of total sequences (Figure 6B). Importantly, this taxon is no longer a prominent population post *T. trichiura* treatment. A single operational taxonomic unit (OTU), most closely related to plastids from plant organisms (*Chloroplast: Streptophyta*), constituted 99.2–99.6% of sequences from the *Cyanobacteria* phyla. BLASTN analysis of the sequence against the nr (NCBI) nucleotide database confirmed sequence identity with *Pinus* chloroplast.

To further identify bacterial clades with statistically significant differences between control, pre-treatment, and post-treatment samples, we used the LEfSe method [32] for comparison between these groups (Figure 7 and S6). By defining pre-treatment and post-treatment samples as two classes of microbial communities, we found that Tenericutes and Bacteroidetes are more abundant in control and post-treatment samples (consistent with the PCoA plot) whereas the unclassified bacteria taxon ZB2 appears to be slightly enriched in pre-treatment samples (Figure 7A–C). When we compared control with post-treatment samples (Figure 7D and S6), we found that Tenericutes is the only taxon more abundant in post-treatment samples, indicating that it could be induced in response to *T. trichiura* treatment.

Discussion

The data presented here suggest that ICD in juvenile rhesus macaques is an IBD-like disease in which the mucosal barrier is compromised, allowing increased bacterial attachment that contributes to persistent inflammation and dysbiosis of the mucosal microbiota. This study revealed that *T. trichiura* treatment induces a T_H2-type immune response in the intestinal mucosa of ICD subjects that was associated with symptomatic improvement. This positive clinical response was inversely correlated with cellular markers of mucosal T cell inflammation, such as Ki67$^+$ T cells. In contrast to the T_H2-type response, T_{reg} expansion was noted under conditions of mucosal inflammation and was reduced by *T. trichiura* treatment, suggesting that the presence of T_{regs} in the intestinal tract is more indicative of ongoing intestinal inflammation than of helminth exposure. Based on these results, we

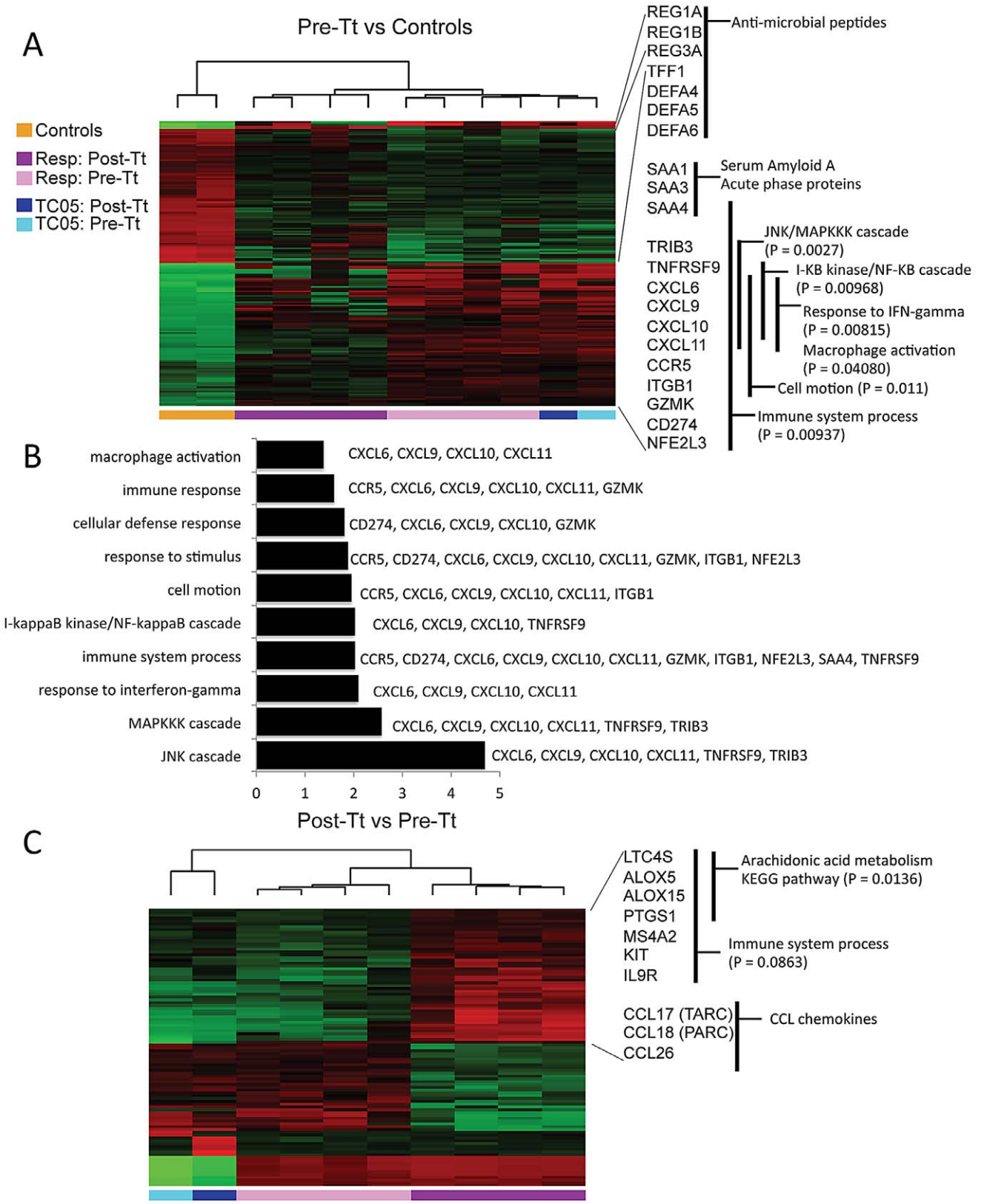

Figure 3. Transcriptional profiling of colon biopsies by macaque whole genome oligonucleotide microarrays. RNA was isolated from pinch biopsies collected during colonoscopies for microarray analysis. Hierarchical clustering analysis of samples and genes based on the expression levels of genes differentially expressed (B>0) between (**A**) pre-treatment colitis samples and healthy controls, where each column represents an individual subject and each row represents a single gene. Black indicates median levels of expression; red, greater than median expression; green, less than median expression. Colored horizontal bars indicate the clustering of samples collected from healthy controls (Controls, orange), clinical

responders [pre-treatment (Resp: Pre-Tt, light purple) and post-treatment (Resp: Post-Tt, dark purple)], and subject TC05 [pre-treatment (TC05: Pre-Tt, light blue) and post-treatment (TC05: Post-Tt, dark blue)]. Representative genes are listed in the biological processes that are overrepresented. (**B**) GO analyses identified biological processes up-regulated in pre-treatment colitis samples. *X* axis indicates the amount of statistical significance [as $-\log(P)$] in enrichment for the indicated biological process, with the up-regulated genes in this process listed. (**C**) Hierarchical clustering analysis of samples and genes based on the expression levels of genes differentially expressed (B>0) between colitis samples before and after *T. trichiura* treatment. The complete list of genes for (A) is shown in Figure S2 and Table S1. The complete list of genes for (C) is shown in Figure S3 and Table S2.
doi:10.1371/journal.ppat.1003000.g003

speculate that *T. trichiura* promotes mucosal healing in the setting of ICD by activating mucus production and epithelial cell turnover, aspects of T_H2-type immunity aimed at expelling the parasite [9,11,21], thereby reducing the attachment of immunostimulatory bacteria to the colonic epithelium and restoring diversity to the mucosal micobiota (Figure 8). However, additional studies are needed to determine the mechanism of action for *Trichuris*-mediated amelioration of colitis, and functional studies to establish causation would have to be performed in a suitable mouse model to confirm these hypotheses.

One weakness of this study is the absence of a control arm to ensure that the macaques with ICD did not undergo spontaneous remission. Future studies to confirm the findings presented here should have a sham-treated control arm, which would also enable a blinded assessment of stool frequency. The association of clinical improvement with weight gains, which is an objective measure, supports the observation that *T. trichiura* treatment did lead to improvement in symptoms. Additionally, our transcriptional profiling experiments clearly show that clinical improvement is associated with dramatic changes in mucosal gene expression patterns. The number of biopsies that could be collected from these juvenile macaques also limited our study. Histopathological observations that could be correlated with gene expression patterns would have provided additional insights into the relationship between cellular infiltrates and mucosal responses. While ICD shares some similar features with UC, inflammation is typically microscopic and cannot be determined objectively by visual inspection during endoscopy.

The mucosal gene expression patterns (e.g., REG1, REG3, NOS2, TFF1, SAA1, and SAA3) that distinguish ICD and healthy macaques are strikingly similar to signatures observed in microarray studies of UC patients [12,26,33,34] as well as in studies of germ free mice repopulated with various bacterial taxa [35,36], suggesting that a response to gut bacteria may be the predominant driving force for this inflammatory signature. Importantly, differences in gene expression patterns were apparent between the four clinical responders and the single non-responder in this study. Of note, the non-responder showed lower expression of immunoglobulin-related genes (Figure S4), suggesting that the etiology of disease in this animal may have stemmed from a defect in the mucosal B cell compartment, as has been shown previously to precipitate colitis through the absence of regulatory B cells [37]. Recently, MyD88 signaling in B cells was found to prevent the lethal dissemination of intestinal bacteria after dextran sulfate sodium (DSS) treatment in mice [38].

The IL-23, IL-17 and IL-22 network plays a critical role in intestinal homeostasis and IBD pathogenesis [39]. We previously reported that IL-22-producing $CD4^+$ cells were a prominent feature of *T. trichiura* infection in a UC patient. Unfortunately, our efforts to stain for IL-17- and IL-22-producing $CD4^+$ cells from the macaque pinch biopsies were unsuccessful (data not shown). When we investigated the expression levels of the cytokines in these pathways pre- and post-*T. trichiura* treatment, we found no significant trends (Figure S7). Since the role of these cytokines in ICD of macaques is completely unknown, this may represent an important difference with human IBD, but it is difficult to draw any conclusions from these results at the moment.

The effects of *T. trichiura* treatment on improving symptoms of colitis occurred despite the absence of a chronic and active infection. Ova were never detected in fecal samples from any of the macaques, indicating the lack of a patent infection, and adult worms were not seen during the post-treatment colonoscopy. The lack of patency is most likely due to a species barrier, since the *T. trichiura* ova used for inoculation were from a human subject [12]. Notably, this parallels the use of *T. suis* ova (TSO) as a therapeutic intervention in human subjects with autoimmune diseases, which

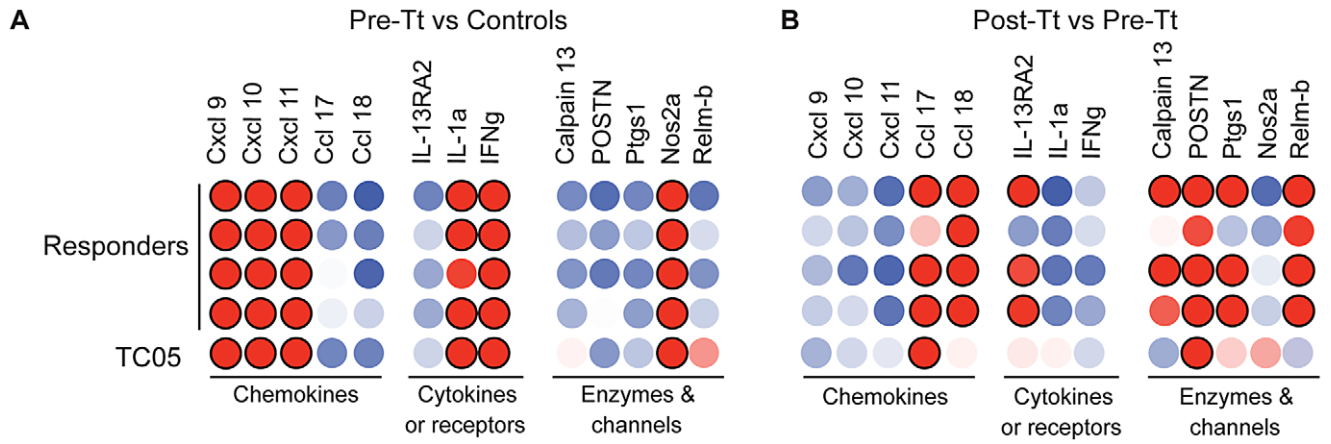

Figure 4. Real-time PCR verification of genes differentially expressed between groups. (**A**) Expression levels of genes in pre-treatment (Pre-Tt) colitis subjects are shown relative to the average expression of samples from healthy controls. Red/pink spots denote higher expression and blue spots represent lower expression; differential expression increases with spot intensity. Red spots with black borders represent >10-fold higher expression. (**B**) Expression levels of genes for samples taken post-treatment (Post-Tt) for each subject are shown relative to pre-treatment levels from the same subject.
doi:10.1371/journal.ppat.1003000.g004

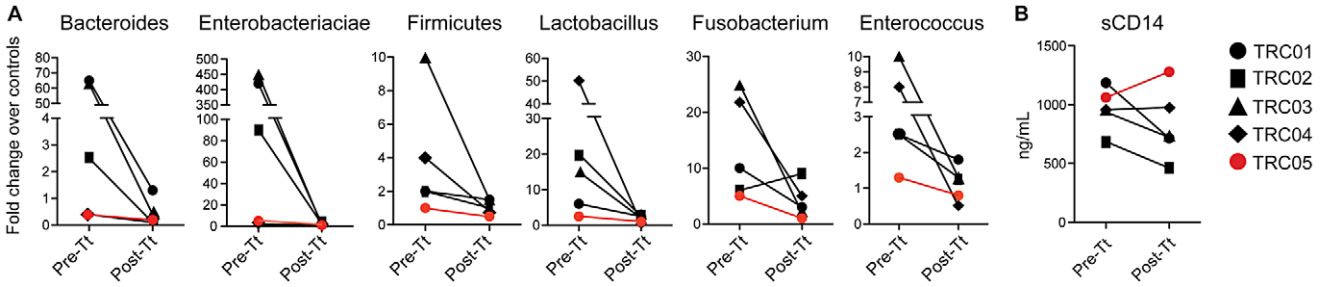

Figure 5. *T. trichiura* treatment reduces bacterial attachment to the colonic mucosa. (**A**) DNA samples harvested from colon biopsies taken pre-treatment (Pre-Tt) and post-treatment (Post-Tt) were analyzed by quantitative PCR for the abundance of bacterial taxa based on specific primers for 16S rRNA sequences. Abundance is expressed as a fold-change above the average value of healthy controls. Subject TC05 is shown in red. (**B**) Plasma levels of soluble CD14 were measured by ELISA.
doi:10.1371/journal.ppat.1003000.g005

is dependent on a species barrier to eliminate the parasites after dosing. After hatching, *Trichuris* larvae molt several times in the intestines before maturing into adult worms. Thus, the larval stages could have elicited a mucosal response leading to a positive clinical outcome. The absence of egg production does not preclude the presence of adult forms or mature larval forms, although none were observed during the endoscopies. Despite the absence of adult forms in humans, TSO clearly induces a strong T_H2 response in treated subjects, as indicated by increased serum IL-4, eosinophilia, and IgE antibodies [40,41]. Although we did not detect more IL-4-producing $CD4^+$ T cells by intracellular cytokine staining in post-treatment PBMCs, this is not indicative that a systemic Th2 response was absent in the macaques. In our previous study [12], responses in PBMCs could only be detected after antigen-specific expansion of $CD4^+$ cells with *T. trichiura* antigen. We propose that the treatment of colitis (but not necessarily other autoimmune diseases) with *Trichuris sp.* may be more dependent on a T_H2 response than immunoregulation. Since we did not detect ova in the feces of the treated macaques, it is also possible that the clinical improvements were spontaneous and not related to *T. trichiura* treatment. However, we find this unlikely since the T_H2 response in the intestinal mucosa at a cellular and molecular level is remarkably consistent among all of the treated macaques.

It is important to note the changes in absolute bacterial quantities as well as the composition of mucosal microbiota following helminth exposure. With both measures, post-treatment samples were much more similar to samples from healthy controls. Perhaps the most consistent observation made in studies on the microbiota of IBD patients is the overall reduction in microbial diversity [23]. There is also reduced diversity of the intestinal microbiota in rhesus macaques with colitis, as noted previously [25] as well as in this study, supporting the use of rhesus macaques with ICD as a preclinical model for IBD.

We noted a striking expansion of Cyanobacteria in three ICD subjects, which disappeared post-treatment. Cyanobacteria have been previously noted to reside in the intestinal tract of mice and humans [42] as well as that of macaques [25]. However, there have not been any previous reports, including studies on the mucosal microbiota from IBD patients [26], where this taxon has represented an abundance of up to 32.9% of 16S sequences. This expansion may reflect a unique environment on the intestinal mucosa of juvenile rhesus monkeys with chronic diarrhea. Notably, a recent publication (including data from the Human Microbiome Project) indicated that, in healthy human beings, the taxon Cyanobacteria:Chloroplast:Streptophyta was enriched in non-mucosal sites relative to mucosal body sites and also enriched under conditions with high oxygen availability [32]. Like *Salmonella typhimurium* [43], perhaps the activation of neutrophils to produce reactive oxygen species favors the expansion of a Cyanobacterium more adapted to an aerobic environment or to alterations in redox conditions. It is also quite possible that these sequences are merely a representation of plant organisms in poorly digested food, which could be more abundantly attached to the mucosa of monkeys suffering from diarrhea.

Since Bacteroidetes is the most predominant phylum in the normal gut, the reduction in proportional abundance in ICD subjects may reflect an expansion of non-Bacteroidetes phyla amongst the mucosal microbiota during ICD. Indeed, quantification of absolute Bacteroidetes abundance by RT-PCR clearly shows a reduction post-treatment. These results reflect a typical problem for this type of 16S compositional data of microbial communities. What is more interesting is the unexpected expansion of Tenericutes after helminth exposure, even relative to control macaques, indicating that bacteria of this phylum could be preferentially expanded in a T_H2-type mucosal environment. Little is known about the role of Tenericutes in the intestinal tract. In one previous study with mice, dextran sodium sulfate (DSS)-driven colitis was shown to decrease the abundance of this phylum [44]. Further studies on the relationship between intestinal helminths and Tenericutes are warranted.

ICD-afflicted juvenile rhesus macaques may represent a useful preclinical model in which to further study the pathology, diagnosis, and treatment of UC in humans under certain circumstances. Most notably, the transcriptional signature of the inflamed mucosa in these macaques closely resembles that of UC patients. Given the prevalence of ICD at primate research centers, this could be an important resource to develop new therapeutics for IBD in humans, especially when addressing the need of a non-rodent model during preclinical testing. However, the costs and ethical issues of using non-human primates may limit the usefulness of this animal model for IBD research towards very specific circumstances when an outbred non-rodent model is required. While very similar, there are also distinct differences between the macaque immune system and the human immune system [45,46] that may limit the use of ICD afflicted rhesus macaques as a model for IBD research.

Our findings describe the immune mechanisms that may mediate the therapeutic effect of *Trichuris sp.* in the setting of colitis and highlight the role of T_H2-type immunity in promoting mucosal repair. Instead of acting through an immunoregulatory mechanism, *Trichuris sp.* may trigger a T_H2-driven expulsion mechanism related to increased mucus production and turnover of epithelial cells, thereby reducing the quantity of attached bacteria among the mucosal microbiota. As part of this process, the

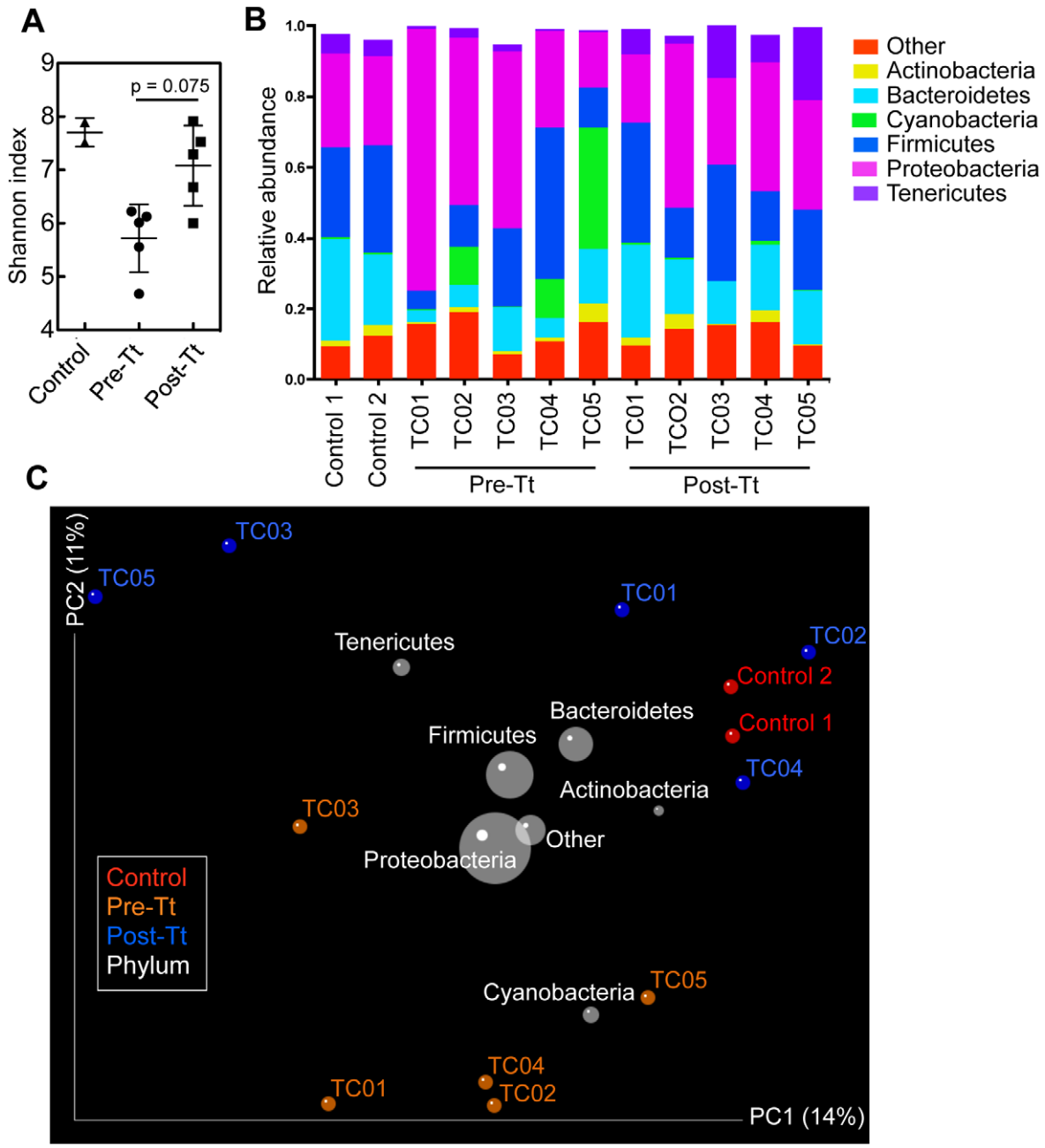

Figure 6. *T. trichiura* treatment influences microbial diversity within samples (α-diversity) and community diversity between samples (β-diversity). (**A**) Shannon diversity of samples from all treatment groups, where each point represents a subject. The average of ten iterations of rarefied subsets of 5422 sequences was used to calculate each Shannon index. The difference between pre- and post-treatment diversity was determined using a Paired Student's t-test ($p = 0.075$). (**B**) Relative abundance of taxonomic groups for each macaque sample. The seven most abundant phyla over all samples are presented. (**C**) The contribution of different taxonomic groups to the separation of samples based on phylogenetic information. Contributions are represented by the size of the circles (grey) overlaid onto a PCoA of unweighted UniFrac distances of macaques pre-treatment (orange), macaques post-treatment (blue), and controls (red).
doi:10.1371/journal.ppat.1003000.g006

dysbiosis observed in the mucosal environment during colitis could also revert back to a normal equilibrium.

Materials and Methods

Ethics statement

This study was carried out in strict accordance with the recommendations in the Guide for the Care and Use of Laboratory Animals of the National Institutes of Health. The use and care of all animals followed policies and guidelines established by the University of California, Davis Institutional Animal Care and Use Committee (IACUC) and CNPRC (Animal Welfare Assurance #A3433-01). The protocol for this trial was approved by the University of California, Davis IACUC. Veterinary care was provided to all animals in order to minimize pain and distress. The California National Primate Research Center (CNPRC), which

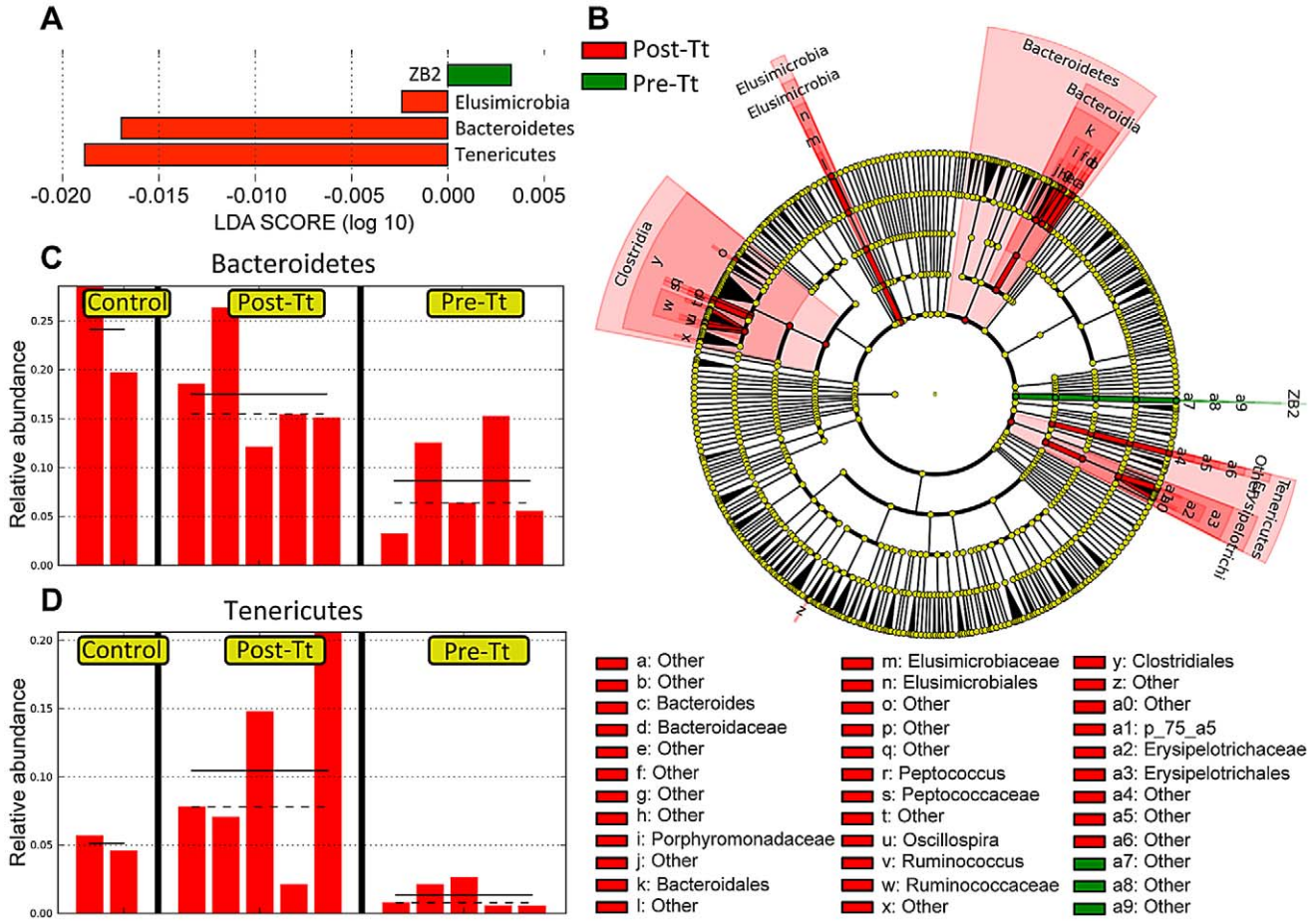

Figure 7. *T. trichiura* treatment recovers several microbial clades reduced in colitic macaques. Utilizing the LEfSe visualization modules and analytical tools, pre-treatment and post-treatment samples were assigned as classes for comparison. (**A**) Histogram of LDA scores computed for features differentially abundant between macaques pre- and post-treatment. (**B**) Cladogram illustrating the taxonomic representation of bacterial taxa with different abundance values in macaques pre- and post-treatment, as determined by LEfSe. Taxa that are more abundant in post-treatment samples are illustrated in red and taxa that are more abundant in pre-treatment samples are illustrated in green. Yellow circles delineate non-significant taxa (**C, D**) Histograms of relative abundances of *Bacteroidetes* (**C**) and of *Tenericutes* (**D**) in control macaques and macaques, pre- and post-treatment.
doi:10.1371/journal.ppat.1003000.g007

houses over 5,000 nonhuman primates, is a part of the National Primate Research Centers Program and is accredited by the Association for the Assessment and Accreditation of Laboratory Animal Care, International (AAALAC). All animal facilities are maintained in compliance with United States Department of Agriculture specifications. Rhesus macaques are maintained in small or large social groups.

Subject recruitment and clinical monitoring

All animals were housed indoors at the CNPRC. ICD cases were identified by recurrent episodes of diarrhea (during 45 or more days in a 90 day period) without evidence for (or a history of) known causes of infectious colitis, as demonstrated by three negative cultures for bacterial pathogens and negative stool examination and immunofluorescence assays for protozoan and helminthic parasites. The diarrhea was refractory to antibiotic and antiparasitic treatment. Animals were weighed every 8–14 days and their stool evaluated according to a standardized four-point scale for fecal consistency (Figure 1).

Collection of colonic biopsies and peripheral blood

Animals were fasted for 36 hours prior to colonoscopy and 30 mL/kg of polyethylene glycol-electrolyte solution (PEG-ES; GoLYTELY brand) was provided twice the day before the procedure by mixing 67 gm with 1 liter of citrus-flavored water (Tang, Kraft Foods, Northfield, IL) and making the solution available for the animals to drink by a hanging bottle in the cage. Blood was collected by venipuncture into citrate tubes prior to colonoscopy. Five pinch biopsies were collected during colonoscopy from the proximal ascending colon. Three biopsies were collected into culture media for *ex vivo* analysis and two biopsies were collected into RNAlater (Qiagen) for nucleic acid extraction.

Flow cytometric analysis of biopsies and peripheral blood

Colon biopsy specimens were treated with 0.25 mg/ml collagenase type II (Sigma-Aldrich) for 30 minutes with constant shaking at room temperature. Digested tissue was dispersed over a 70-micron nylon mesh filter. Cell suspensions were washed twice

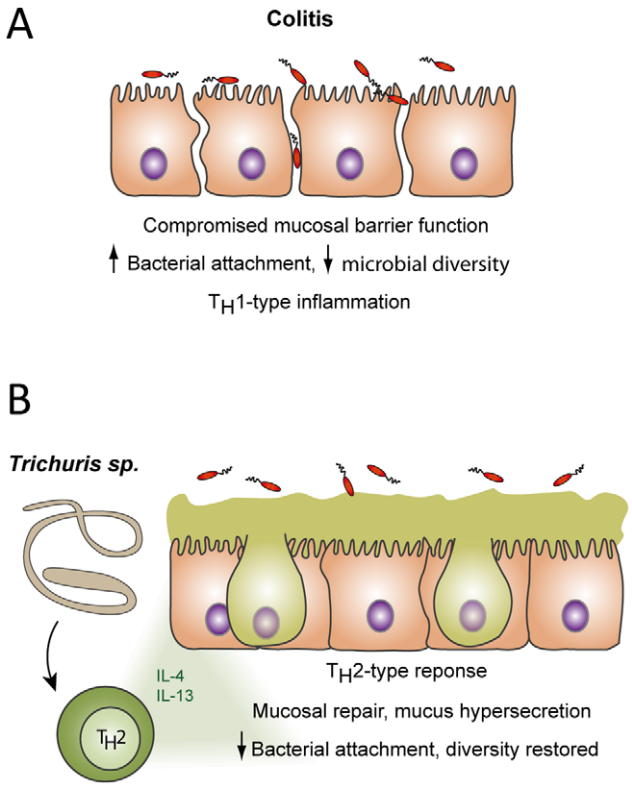

Figure 8. Working model of the immunologic mechanisms underlying the amelioration of colitis in the setting of *Trichuris sp. treatment.* (**A**) Colitis is driven by a T_H1-type inflammatory response to increased bacterial attachment and dysbiosis at the mucosal epithelium as a result of compromised barrier function. (**B**) *Trichuris sp.* elicits a mucosal T_H2-type response (including the canonical cytokines IL-4 and IL-13) that promotes mucosal wound healing and mucus production. These functions reduce bacterial attachment and restore microbial homeostasis, removing the inflammatory stimulus.
doi:10.1371/journal.ppat.1003000.g008

with RPMI containing 15% fetal calf serum. Whole blood was collected into ACD-containing tubes (BD Biosciences) and PBMC were isolated by density centrifugation. Biopsy cells and PBMC (1×10^6) were resuspended in 200 µl of complete R-10 [RPMI 1640 medium (Invitrogen) supplemented with 10% fetal calf serum (Hyclone), 50 U/ml penicillin, 50 µg/ml streptomycin, and 2 mM L-glutamine], and stimulated with phorbol myristate acetate (10 ng/ml) and ionomycin (1 µg/ml) in the presence of brefeldin A (GolgiPlug, BD Pharmingen) for five hours at 37°C. For biopsy cells, amphotericin B (Gibco) was also added to the culture media. Cell surface staining and intracellular cytokine staining were performed with Fix/Perm and PermWash solutions from BD and eBioscience, according to the manufacturer's instructions.

Microarray analysis of biopsy samples

Biopsies were collected into RNAlater (Qiagen) and homogenized in TRIzol (Invitrogen). RNA was collected in the aqueous extraction phase and column purified using an RNeasy kit (Qiagen). Sample preparation, labeling, and array hybridizations were performed according to standard protocols from the UCSF Shared Microarray Core Facilities and Agilent Technologies (http://www.arrays.ucsf.edu and http://www.agilent.com). Total RNA quality was assessed using a Pico Chip on an Agilent 2100 Bioanalyzer (Agilent Technologies, Palo Alto, CA). RNA was amplified and labeled with Cy3-CTP using the Agilent low RNA input fluorescent linear amplification kits following the manufacturer's protocol (Agilent). Labeled cRNA was assessed using the Nandrop ND-100 (Nanodrop Technologies, Inc., Wilmington DE) and equal amounts of Cy3 labeled target were hybridized to Agilent Rhesus Macaque (V2) whole genome 4x44K Ink-jet arrays (Agilent). Hybridizations were performed for 14 hours, according to the manufacturer's protocol (Agilent). Arrays were scanned using the Agilent microarray scanner (Agilent) and raw signal intensities were extracted with Feature Extraction v10.1 software (Agilent). Each data set was normalized using the *quantile* normalization method [47] with no background subtraction. A one-way ANOVA linear model was fit to the comparison to estimate the mean M values and calculated B statistic, false discovery rate and p-value for each gene for the comparison of interest. All procedures were carried out using functions in the R package. For DAVID [48] and PANTHER [49] pathway analyses, EnsEMBL and Genbank accession numbers associated with significantly different *M. mulatta* genes were converted to official gene symbols, along with a background list consisting of all genes used as input to the analyses. Functional annotation charts were generated using the default parameters. Reported p-values are Bonferroni-corrected. For these analyses, the human pathways and ontologies were used as they are more fully developed than those available for macaques.

RT-PCR analysis of RNA and DNA from colon biopsies

Tissue samples were homogenized in TRIzol (Invitrogen). RNA was collected in the aqueous extraction phase, and DNA was harvested from the interphase and phenol-chloroform organic phase. RNA was column purified using an RNeasy kit (Qiagen). cDNA was generated using an Omniscript Reverse Transcription kit (Qiagen) with oligo-dT primers in the presence of RNasin Plus RNase inhibitor (Promega). DNA was collected by ethanol precipitation and washed according to the manufacturer's instructions. PCR reactions were carried out with Taqman primer/probe sets (Applied Biosystems) in a StepOne Plus machine (Applied Biosystems). The abundances of major intestinal bacterial groups were measured by qPCR of extracted DNA, using the MyIQ single-color real-time PCR detection system (Bio-Rad, Hercules, CA) and group-specific 16S rRNA gene primers that have been previously published and verified [50]. Samples were normalized to controls and eubacteria.

Soluble CD14 analysis

Plasma sCD14 levels were measured using the Quantikine ELISA kit (R&D Systems; Minneapolis, Minnesota, USA), as described in the manufacturer's protocol. Plasma samples were diluted 1/500 and run in duplicate.

16S rRNA analyses

DNA samples isolated from pinch biopsies were PCR amplified for sequencing through a validated protocol [31]. The V4 region of the 16S rRNA gene was amplified with region specific barcoded primers [51] and sequenced on a MiSeq sequencer [31] along with other barcoded samples. Reads shorter than 140 bp were discarded. The QIIME suite of analysis tools was used to filter and analyze the sequence data [52]. Sequences were assigned to OTUs with a threshold of 97% pair-wise identity and then classified taxonomically using the Ribosomal Database Project (RDP) classifier. A representative sequence for each OTU was aligned using PyNAST and used to build a phylogenetic tree for α-diversity and β-diversity measurements. Alpha rarefaction was performed using the Shannon index and phylogenetic diversity. Beta diversity was calculated in QIIME, using default metrics of

weighted and unweighted UniFrac distances between samples, and visualized using Principal Coordinate Analysis (PCoA) plots and Unweighted Pair Group Method with Arithmetic Mean (UPGMA) trees. Relative abundance of microbial phyla was determined in QIIME by grouping OTUs by macaque sample. To identify significant differences in bacterial taxa between groups, we utilized the linear discriminant analysis (LDA) effect size (LEfSe) algorithm [32] through the Galaxy Framework [53,54] online. LEfSe uses the Kruskal-Wallis (KW) sum-rank test to detect features with significantly different abundances between classes, and performs LDA to estimate the effect size of each differentially abundant feature. So that we could recover all features detected by the KW test, we did not set a threshold for LDA in the analysis.

Supporting Information

Figure S1 Spontaneous remission does not occur in untreated juvenile macaques with chronic diarrhea. Fecal consistency scores (FCS) were based on a standardized 4-point scale; 1 = Well-formed, normal; 1.5 = Normal to semi-solid; 2 = Semi-solid to normal; 2.5 = Semi-solid; 3 = Semi-solid to liquid; 3.5 = Liquid to semi-solid; 4 = Liquid. Semi solid stool is defined as "porridge-like" or able to be picked up with a fork. Data is shown as the average and SEM of N = 7 subjects.
(TIFF)

Figure S2 Hierarchical clustering of genes differentially expressed in colon biopsies between colitis subjects [before (Pre) and after (Post) *T. trichiura* treatment] and healthy controls (Cont) as shown in Figure 1, with gene symbols listed.
(TIF)

Figure S3 Hierarchical clustering of genes differentially expressed in colon biopsies following *T. trichiura* treatment in clinical responders (R) and subject TC05 (NR) as shown in Figure 1, with gene symbols listed.
(TIF)

Figure S4 Hierarchical clustering of genes differentially expressed between clinical responders (R) and subject TC05 (NR) pre-treatment, with gene symbols listed. Probe ID's are shown where gene symbols are not available. Additional annotation indicates probes that represent Immunoglobulin genes that are down regulated in expression in subject TC05 (NR).
(TIF)

Figure S5 *T. trichiura* treatment influences microbial diversity within samples (α-diversity) and community diversity between samples (β-diversity). (**A, B**) Rarefaction plots of Shannon diversity (**A**) and phylogenetic diversity (**B**). The average of ten iterations of rarefied subsets was used to calculate each metric. Metrics are averaged across macaques within each treatment and error bars represent the standard deviation. (**C**) Phylogenetic diversity of each macaque sample, calculated by the average of ten iterations of rarefied subsets of 5422 sequences. The difference between pre- and post-treatment diversity was determined using a Paired Student's t-test ($p = 0.178$). (**D, E**) UPGMA trees of unweighted UniFrac (**D**) and weighted UniFrac (**E**). Branch colors: macaques pre-treatment (orange), macaques post-treatment (blue), and controls (red).
(TIF)

Figure S6 *T. trichiura* treatment increases the relative abundance of bacteria from the phyla *Tenericutes* in treated macaques compared to control healthy macaques. Utilizing LEfSe, post-treatment samples and control samples were assigned as classes for comparison. The cladogram illustrates the taxonomic representation of bacterial taxa with different abundance values in control macaques and post-treatment macaaques. Taxa that are more abundant in control samples are illustrated in red and taxa that are more abundant in post-treatment samples are illustrated in green. Yellow circles delineate non-significant taxa.
(TIF)

Figure S7 Expression of $T_H17/22$ cytokine genes from pinch biopsies pre-treatment (Pre-Tt) and post-treatment (Post-Tt) showed no significant trends. Expression levels of genes in pre-treatment (Pre-Tt) and post-treatment (Post-Tt) colitis subjects were extracted from the microarray dataset. Expression levels of IL-17 were confirmed by RT-PCR (data not shown). Samples from subject TC05 are shown in red.
(TIF)

Table S1 List of genes differentially expressed in colon biopsies between colitis subjects and healthy controls. Genes most highly expressed in colitis subjects are listed at the top. FDR, false discovery rate.
(PDF)

Table S2 List of genes differentially expressed in colon biopsies from colitis subjects before and after *T. trichiura* treatment. Genes most highly expressed following treatment are listed at the top. FDR, false discovery rate.
(PDF)

Table S3 List of genes differentially expressed in colon biopsies between clinical responders (R) and subject TC05 (NR) pre-treatment with *T. trichiura*. Genes most highly expressed in the non-responding subject TC05 are listed at the top. FDR, false discovery rate.
(PDF)

Acknowledgments

We thank K.C. Lim for parasitology assistance and expertise. We thank R. Dunham, and the UCSF Genomics Core for assistance in experimental design and data analysis. We thank members of the Earth Microbiome Project at Argonne National Laboratories for microbial sequencing. We thank T. Traill for assistance in clinical scoring.

Author Contributions

Conceived and designed the experiments: MJB FY NWL JMM PL. Performed the experiments: MJB AA BK JM UMG JML IVC. Analyzed the data: MJB JM KEW CCK FY NWL JMM PL. Wrote the paper: MJB KEW JMM PL.

References

1. Weinstock JV (2006) Helminths and mucosal immune modulation. Ann N Y Acad Sci 1072: 356–364.
2. Summers RW, Elliott DE, Urban JF, Jr., Thompson R, Weinstock JV (2005) Trichuris suis therapy in Crohn's disease. Gut 54: 87–90.

3. Summers RW, Elliott DE, Urban JF, Jr., Thompson RA, Weinstock JV (2005) Trichuris suis therapy for active ulcerative colitis: a randomized controlled trial. Gastroenterology 128: 825–832.
4. Smith P, Mangan NE, Walsh CM, Fallon RE, McKenzie AN, et al. (2007) Infection with a helminth parasite prevents experimental colitis via a macrophage-mediated mechanism. J Immunol 178: 4557–4566.
5. Elliott DE, Li J, Blum A, Metwali A, Qadir K, et al. (2003) Exposure to schistosome eggs protects mice from TNBS-induced colitis. Am J Physiol Gastrointest Liver Physiol 284: G385–391.
6. Elliott DE, Setiawan T, Metwali A, Blum A, Urban JF, Jr., et al. (2004) Heligmosomoides polygyrus inhibits established colitis in IL-10-deficient mice. Eur J Immunol 34: 2690–2698.
7. Khan WI, Blennerhasset PA, Varghese AK, Chowdhury SK, Omsted P, et al. (2002) Intestinal nematode infection ameliorates experimental colitis in mice. Infect Immun 70: 5931–5937.
8. Maizels RM, Yazdanbakhsh M (2003) Immune regulation by helminth parasites: cellular and molecular mechanisms. Nat Rev Immunol 3: 733–744.
9. Allen JE, Maizels RM (2011) Diversity and dialogue in immunity to helminths. Nat Rev Immunol 11: 375–388.
10. Allen JE, Wynn TA (2011) Evolution of Th2 immunity: a rapid repair response to tissue destructive pathogens. PLoS Pathog 7: e1002003.
11. Wolff MJ, Broadhurst MJ, Loke P (2012) Helminthic therapy: improving mucosal barrier function. Trends Parasitol 28: 187–194.
12. Broadhurst MJ, Leung JM, Kashyap V, McCune JM, Mahadevan U, et al. (2010) IL-22+ CD4+ T cells are associated with therapeutic trichuris trichiura infection in an ulcerative colitis patient. Sci Transl Med 2: 60ra88.
13. Gaze S, McSorley HJ, Daveson J, Jones D, Bethony JM, et al. (2012) Characterising the mucosal and systemic immune responses to experimental human hookworm infection. PLoS Pathog 8: e1002520.
14. McSorley HJ, Gaze S, Daveson J, Jones D, Anderson RP, et al. (2011) Suppression of inflammatory immune responses in celiac disease by experimental hookworm infection. PLoS One 6: e24092.
15. Daveson AJ, Jones DM, Gaze S, McSorley H, Clouston A, et al. (2011) Effect of hookworm infection on wheat challenge in celiac disease–a randomised double-blinded placebo controlled trial. PLoS One 6: e17366.
16. Elmore DB, Anderson JH, Hird DW, Sanders KD, Lerche NW (1992) Diarrhea rates and risk factors for developing chronic diarrhea in infant and juvenile rhesus monkeys. Lab Anim Sci 42: 356–359.
17. Blackwood RS, Tarara RP, Christe KL, Spinner A, Lerche NW (2008) Effects of the macrolide drug tylosin on chronic diarrhea in rhesus macaques (Macaca mulatta). Comp Med 58: 81–87.
18. Sestak K, Merritt CK, Borda J, Saylor E, Schwamberger SR, et al. (2003) Infectious agent and immune response characteristics of chronic enterocolitis in captive rhesus macaques. Infect Immun 71: 4079–4086.
19. Mohan M, Aye PP, Borda JT, Alvarez X, Lackner AA (2007) Gastrointestinal disease in simian immunodeficiency virus-infected rhesus macaques is characterized by proinflammatory dysregulation of the interleukin-6-Janus kinase/signal transducer and activator of transcription3 pathway. Am J Pathol 171: 1952–1965.
20. Walk ST, Blum AM, Ewing SA, Weinstock JV, Young VB (2010) Alteration of the murine gut microbiota during infection with the parasitic helminth Heligmosomoides polygyrus. Inflamm Bowel Dis 16: 1841–1849.
21. Artis D, Grencis RK (2008) The intestinal epithelium: sensors to effectors in nematode infection. Mucosal Immunol 1: 252–264.
22. Hayes KS, Bancroft AJ, Goldrick M, Portsmouth C, Roberts IS, et al. (2010) Exploitation of the intestinal microflora by the parasitic nematode Trichuris muris. Science 328: 1391–1394.
23. Clemente JC, Ursell LK, Parfrey LW, Knight R (2012) The impact of the gut microbiota on human health: an integrative view. Cell 148: 1258–1270.
24. Kau AL, Ahern PP, Griffin NW, Goodman AL, Gordon JI (2011) Human nutrition, the gut microbiome and the immune system. Nature 474: 327–336.
25. McKenna P, Hoffmann C, Minkah N, Aye PP, Lackner A, et al. (2008) The macaque gut microbiome in health, lentiviral infection, and chronic enterocolitis. PLoS Pathog 4: e20.
26. Lepage P, Hasler R, Spehlmann ME, Rehman A, Zvirbliene A, et al. (2011) Twin study indicates loss of interaction between microbiota and mucosa of patients with ulcerative colitis. Gastroenterology 141: 227–236.
27. Kalinski P (2012) Regulation of immune responses by prostaglandin E2. J Immunol 188: 21–28.
28. Garrett WS, Gordon JI, Glimcher LH (2010) Homeostasis and inflammation in the intestine. Cell 140: 859–870.
29. Xavier RJ, Podolsky DK (2007) Unravelling the pathogenesis of inflammatory bowel disease. Nature 448: 427–434.
30. Sandler NG, Wand H, Roque A, Law M, Nason MC, et al. (2011) Plasma levels of soluble CD14 independently predict mortality in HIV infection. J Infect Dis 203: 780–790.
31. Caporaso JG, Lauber CL, Walters WA, Berg-Lyons D, Huntley J, et al. (2012) Ultra-high-throughput microbial community analysis on the Illumina HiSeq and MiSeq platforms. ISME J 6: 1621–4.
32. Segata N, Izard J, Waldron L, Gevers D, Miropolsky L, et al. (2011) Metagenomic biomarker discovery and explanation. Genome Biol 12: R60.
33. Noble CL, Abbas AR, Cornelius J, Lees CW, Ho GT, et al. (2008) Regional variation in gene expression in the healthy colon is dysregulated in ulcerative colitis. Gut 57: 1398–1405.
34. Toedter G, Li K, Marano C, Ma K, Sague S, et al. (2011) Gene expression profiling and response signatures associated with differential responses to infliximab treatment in ulcerative colitis. Am J Gastroenterol 106: 1272–1280.
35. Cash HL, Whitham CV, Behrendt CL, Hooper LV (2006) Symbiotic bacteria direct expression of an intestinal bactericidal lectin. Science 313: 1126–1130.
36. Ivanov, II, Atarashi K, Manel N, Brodie EL, Shima T, et al. (2009) Induction of intestinal Th17 cells by segmented filamentous bacteria. Cell 139: 485–498.
37. Mizoguchi A, Bhan AK (2006) A case for regulatory B cells. J Immunol 176: 705–710.
38. Kirkland D, Benson A, Mirpuri J, Pifer R, Hou B, et al. (2012) B cell-intrinsic MyD88 signaling prevents the lethal dissemination of commensal bacteria during colonic damage. Immunity 36: 228–238.
39. Maloy KJ, Powrie F (2011) Intestinal homeostasis and its breakdown in inflammatory bowel disease. Nature 474: 298–306.
40. Bager P, Arnved J, Ronborg S, Wohlfahrt J, Poulsen LK, et al. (2010) Trichuris suis ova therapy for allergic rhinitis: a randomized, double-blind, placebo-controlled clinical trial. J Allergy Clin Immunol 125: 123–130 e121–123.
41. Fleming JO, Isaak A, Lee JE, Luzzio CC, Carrithers MD, et al. (2011) Probiotic helminth administration in relapsing-remitting multiple sclerosis: a phase 1 study. Mult Scler 17: 743–754.
42. Ley RE, Backhed F, Turnbaugh P, Lozupone CA, Knight RD, et al. (2005) Obesity alters gut microbial ecology. Proc Natl Acad Sci U S A 102: 11070–11075.
43. Winter SE, Thiennimitr P, Winter MG, Butler BP, Huseby DL, et al. (2010) Gut inflammation provides a respiratory electron acceptor for Salmonella. Nature 467: 426–429.
44. Nagalingam NA, Kao JY, Young VB (2011) Microbial ecology of the murine gut associated with the development of dextran sodium sulfate-induced colitis. Inflamm Bowel Dis 17: 917–926.
45. Haigwood NL, Walker CM (2011) Commissioned Paper: Comparison of Immunity to Pathogens in Humans, Chimpanzees, and Macaques. . Chimpanzees in Biomedical and Behavioral Research: Assessing the Necessity Washington (DC): National Academies Press
46. Messaoudi I, Estep R, Robinson B, Wong SW (2011) Nonhuman primate models of human immunology. Antioxid Redox Signal 14: 261–273.
47. Bolstad BM, Irizarry RA, Astrand M, Speed TP (2003) A comparison of normalization methods for high density oligonucleotide array data based on variance and bias. Bioinformatics 19: 185–193.
48. Huang da W, Sherman BT, Lempicki RA (2009) Systematic and integrative analysis of large gene lists using DAVID bioinformatics resources. Nat Protoc 4: 44–57.
49. Thomas PD, Kejariwal A, Campbell MJ, Mi H, Diemer K, et al. (2003) PANTHER: a browsable database of gene products organized by biological function, using curated protein family and subfamily classification. Nucleic Acids Res 31: 334–341.
50. Bouskra D, Brezillon C, Berard M, Werts C, Varona R, et al. (2008) Lymphoid tissue genesis induced by commensals through NOD1 regulates intestinal homeostasis. Nature 456: 507–510.
51. Caporaso JG, Lauber CL, Walters WA, Berg-Lyons D, Lozupone CA, et al. (2011) Global patterns of 16S rRNA diversity at a depth of millions of sequences per sample. Proc Natl Acad Sci U S A 108 Suppl 1: 4516–4522.
52. Caporaso JG, Kuczynski J, Stombaugh J, Bittinger K, Bushman FD, et al. (2010) QIIME allows analysis of high-throughput community sequencing data. Nat Methods 7: 335–336.
53. Goecks J, Nekrutenko A, Taylor J (2010) Galaxy: a comprehensive approach for supporting accessible, reproducible, and transparent computational research in the life sciences. Genome Biol 11: R86.
54. Blankenberg D, Von Kuster G, Coraor N, Ananda G, Lazarus R, et al. (2010) Galaxy: a web-based genome analysis tool for experimentalists. Curr Protoc Mol Biol Chapter 19: Unit 19 10 11–21.

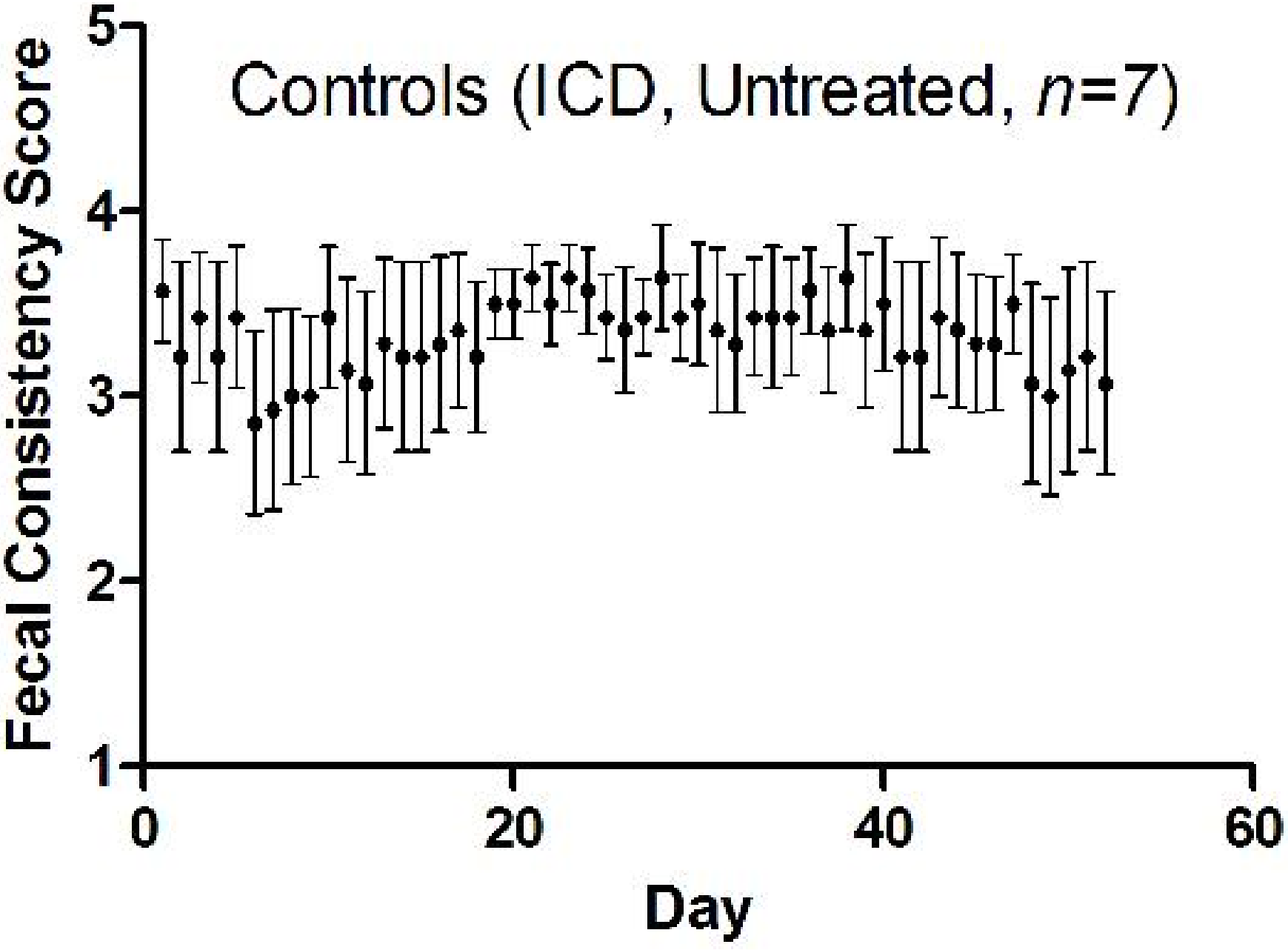
Controls (ICD, Untreated, n=7)
Fecal Consistency Score
5
4
3
2
1
0
20
40
60
Day

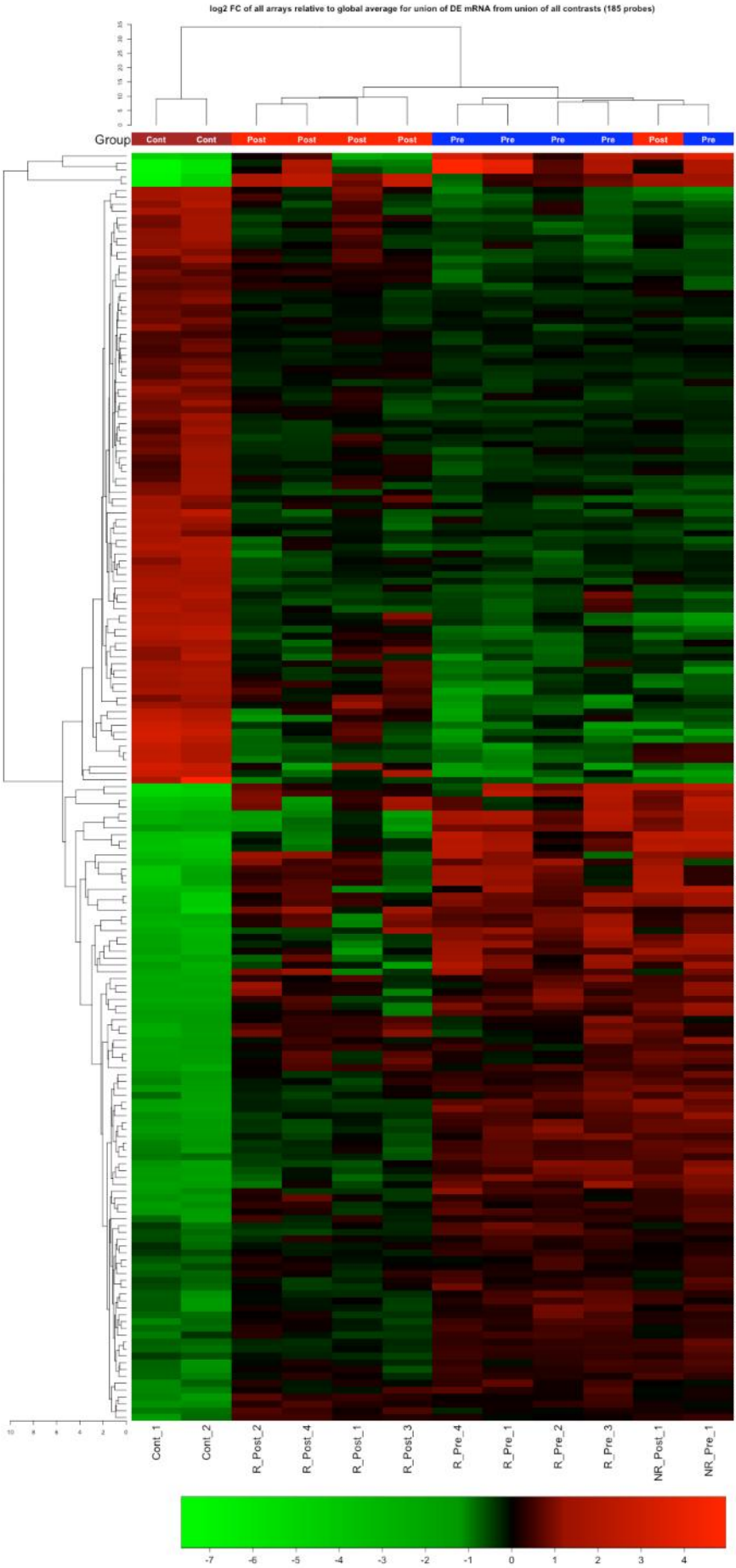
log2 FC of all arrays relative to global average for union of DE mRNA from union of all contrasts (185 probes)
Group
Cont
Cont
Post
Post
Post
Post
Pre
Pre
Pre
Pre
Post
Pre
Cont_1
Cont_2
R_Post_2
R_Post_4
R_Post_1
R_Post_3
R_Pre_4
R_Pre_1
R_Pre_2
R_Pre_3
NR_Post_1
NR_Pre_1
-7
-6
-5
-4
-3
-2
-1
0
1
2
3
4

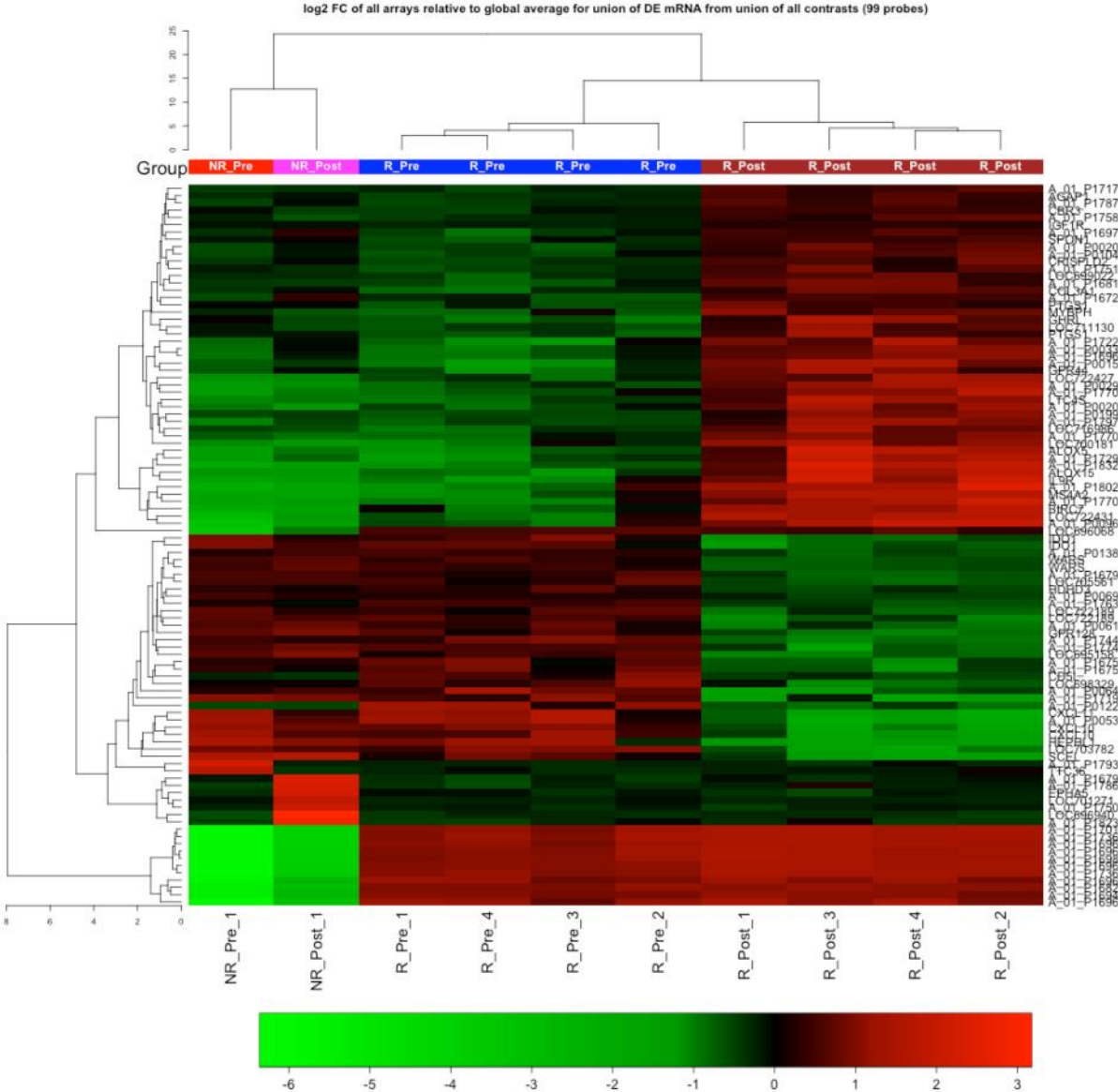
log2 FC of all arrays relative to global average for union of DE mRNA from union of all contrasts (99 probes)
Group
NR_Pre
NR_Post
R_Pre
R_Pre
R_Pre
R_Pre
R_Post
R_Post
R_Post
R_Post
NR_Pre_1
NR_Post_1
R_Pre_1
R_Pre_4
R_Pre_3
R_Pre_2
R_Post_1
R_Post_3
R_Post_4
R_Post_2
-6
-5
-4
-3
-2
-1
0
1
2
3

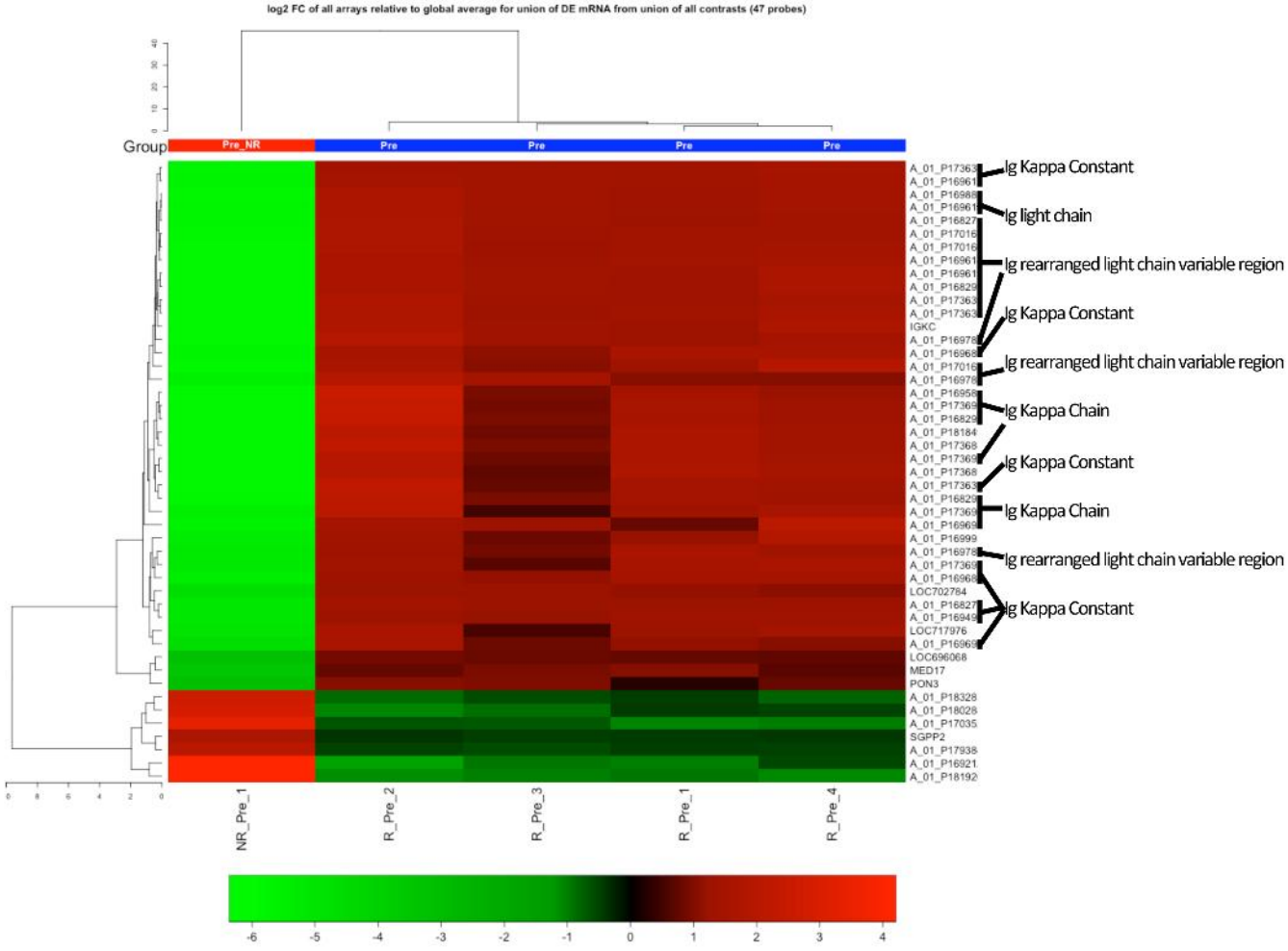
log2 FC of all arrays relative to global average for union of DE mRNA from union of all contrasts (47 probes)
Group
Pre_NR
Pre
Pre
Pre
Pre
A_01_P17363
A_01_P16961
A_01_P16988
A_01_P16961
A_01_P16827
A_01_P17016
A_01_P17016
A_01_P16961
A_01_P16961
A_01_P16829
A_01_P17363
A_01_P17363
IGKC
A_01_P16978
A_01_P16968
A_01_P17016
A_01_P16978
A_01_P16958
A_01_P17369
A_01_P16829
A_01_P18184
A_01_P17368
A_01_P17369
A_01_P17368
A_01_P17363
A_01_P16829
A_01_P17369
A_01_P16969
A_01_P16999
A_01_P16978
A_01_P17369
A_01_P16968
LOC702784
A_01_P16827
A_01_P16949
LOC717976
A_01_P16968
LOC696068
MED17
PON3
A_01_P18328
A_01_P18026
A_01_P17035
SGPP2
A_01_P17938
A_01_P16921
A_01_P18192
Ig Kappa Constant
Ig light chain
Ig rearranged light chain variable region
Ig Kappa Constant
Ig rearranged light chain variable region
Ig Kappa Chain
Ig Kappa Constant
Ig Kappa Chain
Ig rearranged light chain variable region
Ig Kappa Constant
NR_Pre_1
R_Pre_2
R_Pre_3
R_Pre_1
R_Pre_4
-6
-5
-4
-3
-2
-1
0
1
2
3
4

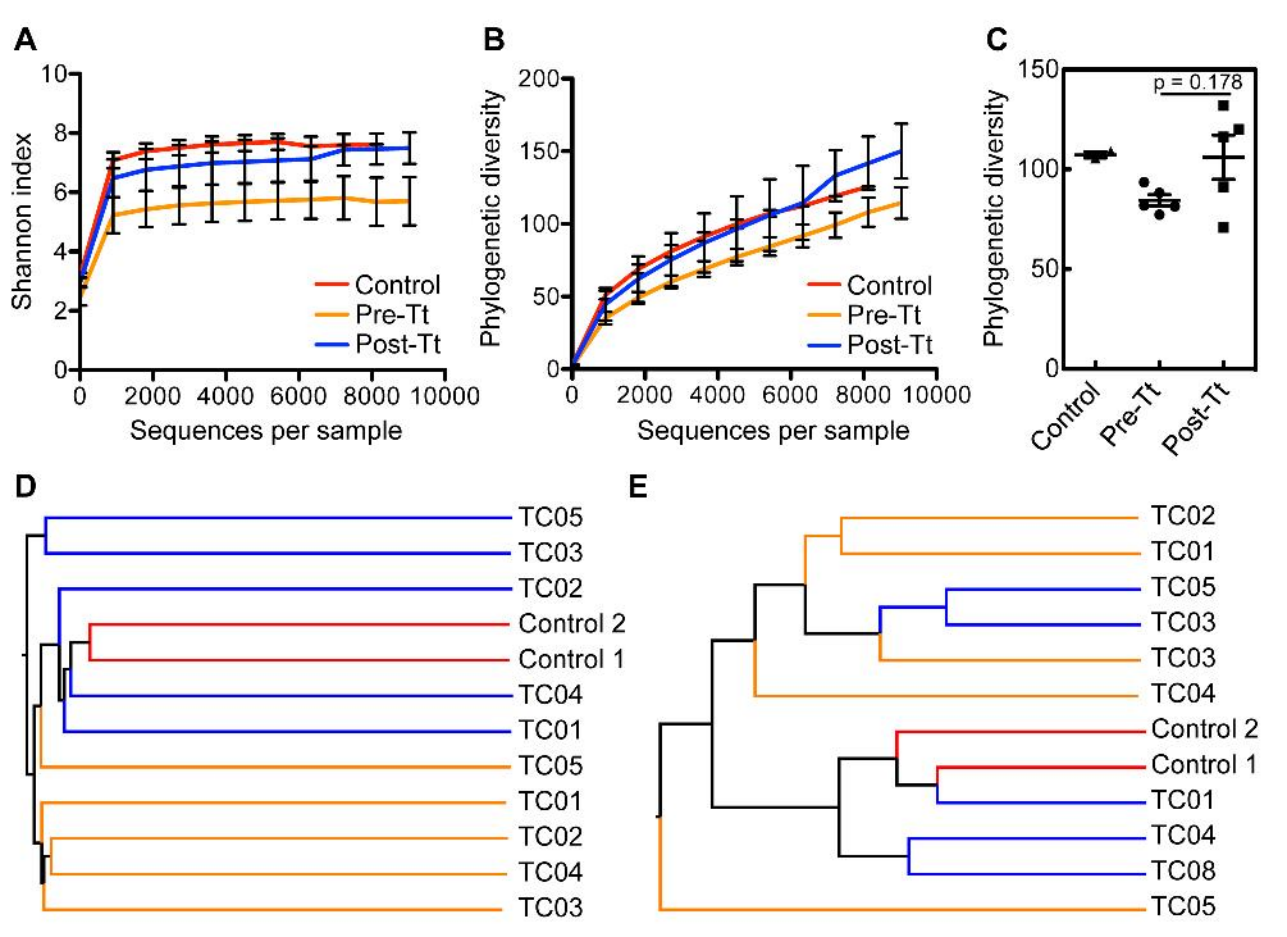
A
Shannon index
Sequences per sample
Control
Pre-Tt
Post-Tt
B
Phylogenetic diversity
Sequences per sample
Control
Pre-Tt
Post-Tt
C
Phylogenetic diversity
p = 0.178
Control
Pre-Tt
Post-Tt
D
TC05
TC03
TC02
Control 2
Control 1
TC04
TC01
TC05
TC01
TC02
TC04
TC03
E
TC02
TC01
TC05
TC03
TC03
TC04
Control 2
Control 1
TC01
TC04
TC08
TC05

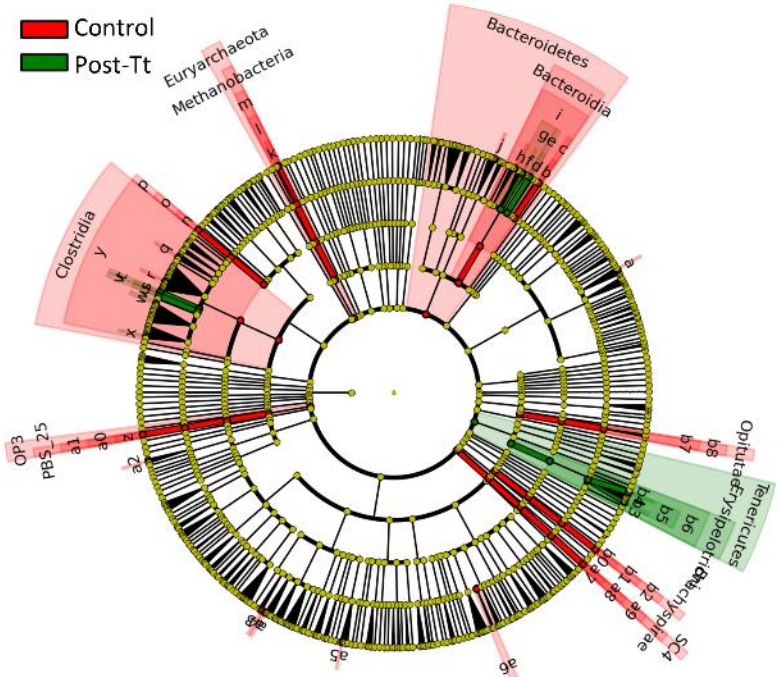

a: Other
b: Other
c: Other
d: Other
e: Other
f: Other
g: Porphyomonadaceae
h: Other
i: Bacteroidales
j: Chryseobacterium
k: Methanobrevibacter
l: Methanobacteriaceae
m: Methanobacteriales
n: Other
o: Turibacteraceae
p: Turicibacterales
q: Finegoldia
r: Lachnospira
s: Other
t: Other
u: Peptococcus
v: Peptococcaceae
w: Other
x: Other
y: Clostridiales
z: Other
a0: Other
a1: Other
a2: Gemmata
a3: Tepidimonas
a4: Other
a5: Methyloversatilis
a6: Coxiellaceae
a7: Other
a8: Other
a9: Other
b0: Brachyspira
b1: Brachyspiraceae

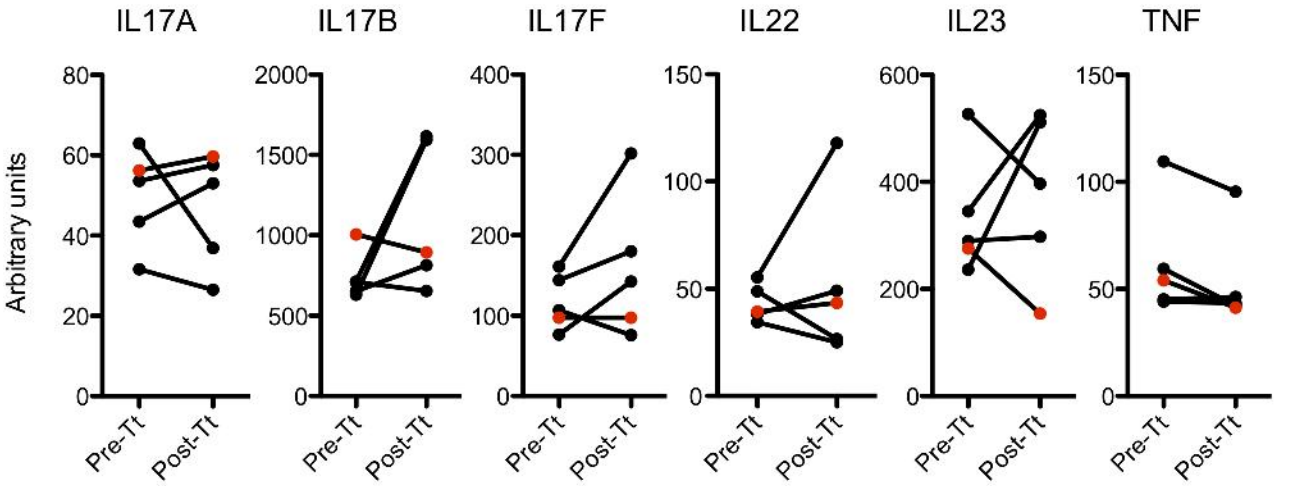
IL17A
IL17B
IL17F
IL22
IL23
TNF
Arbitrary units
80
60
40
20
0
2000
1500
1000
500
400
300
200
100
150
50
600
Pre-Tt
Post-Tt

Table S1

Description	Fold	FDR
ILLUMIGEN_MCQ_46808 Katze_MMJJ Macaca mulatta cDNA clone IBIUW:18836 5' similar to Bases 23 to 794 highly similar to human REG1A (Hs.49407), mRNA sequence [CO581740]	500.00	0.005
Macaca mulatta regenerating islet-derived 1 beta (REG1B), mRNA [NM_001194568]	125.00	0.027
transcobalamin I (vitamin B12 binding protein, R binder family) [Source:HGNC Symbol;Acc:11652] [ENSMMUT00000018989]	83.33	0.002
transcobalamin I (vitamin B12 binding protein, R binder family) [Source:HGNC Symbol;Acc:11652] [ENSMMUT00000018989]	76.92	0.003
PREDICTED: Macaca mulatta serum amyloid A protein-like, transcript variant 1 (LOC694944), mRNA [XM_001086477]	71.43	0.002
Amyloid protein A (Amyloid fibril protein AA) [Source:UniProtKB/Swiss-Prot;Acc:P02738] [ENSMMUT00000015626]	71.43	0.006
PREDICTED: Macaca mulatta nitric oxide synthase 2, inducible, transcript variant 4 (NOS2), mRNA [XM_001106245]	38.46	0.010
PREDICTED: Macaca mulatta nitric oxide synthase 2, inducible, transcript variant 4 (NOS2), mRNA [XM_001106245]	27.03	0.047
Macaca mulatta protease, serine, 2 (trypsin 2) (PRSS2), mRNA [NM_001047120]	22.73	0.041
chitinase 3-like 1 (cartilage glycoprotein-39) [Source:HGNC Symbol;Acc:1932] [ENSMMUT00000012174]	21.74	0.002
chitinase 3-like 1 (cartilage glycoprotein-39) [Source:HGNC Symbol;Acc:1932] [ENSMMUT00000012174]	20.83	0.002
Macaca mulatta dual oxidase maturation factor 2 (DUOXA2), mRNA [NM_001194505]	18.18	0.027
serum amyloid A4, constitutive [Source:HGNC Symbol;Acc:10516] [ENSMMUT00000015624]	17.54	0.046
protease, serine, 2 [Source:RefSeq peptide;Acc:NP_001040585] [ENSMMUT00000041633]	17.54	0.041
small inducible cytokine B11 [Source:RefSeq peptide;Acc:NP_001028122] [ENSMMUT00000029393]	16.39	0.021
ankyrin repeat domain 22 [Source:HGNC Symbol;Acc:28321] [ENSMMUT00000000694]	16.13	0.011
Macaca mulatta chemokine (C-X-C motif) ligand 11 (CXCL11), mRNA [NM_001032950]	15.87	0.010
Macaca mulatta chemokine (C-X-C motif) ligand 9 (CXCL9), mRNA [NM_001032936]	14.93	0.006
Macaca mulatta unknown Fragment [Source:UniProtKB/TrEMBL;Acc:O97682] [ENSMMUT00000029735]	13.89	0.029
Macaca mulatta unknown Fragment [Source:UniProtKB/TrEMBL;Acc:O97682] [ENSMMUT00000029736]	12.35	0.046
succinate receptor 1 [Source:HGNC Symbol;Acc:4542] [ENSMMUT00000002359]	12.20	0.004
Macaca mulatta unknown Fragment [Source:UniProtKB/TrEMBL;Acc:O97682] [ENSMMUT00000029736]	12.20	0.041
Macaca mulatta indoleamine 2,3-dioxygenase 1 (IDO1), mRNA [NM_001077483]	10.10	0.003
Macaca mulatta indoleamine 2,3-dioxygenase 1 (IDO1), mRNA [NM_001077483]	10.00	0.008
annexin A3 [Source:HGNC Symbol;Acc:541] [ENSMMUT00000031250]	8.47	0.041
chemokine (C-X-C motif) ligand 6 (granulocyte chemotactic protein 2) [Source:HGNC Symbol;Acc:10643] [ENSMMUT00000025054]	8.00	0.042
inhibin, beta A [Source:HGNC Symbol;Acc:6066] [ENSMMUT00000019988]	7.58	0.037
Macaca mulatta tripartite motif-containing 5 (TRIM5), mRNA [NM_001032910]	7.52	0.048
EGF-like-domain, multiple 6 [Source:HGNC Symbol;Acc:3235] [ENSMMUT00000031824]	7.19	0.003
C-X-C motif chemokine 10 Precursor (Small-inducible cytokine B10)(10 kDa interferon-gamma-induced protein)(Gamma-IP10)(IP-10) [Source:UniProtKB/Swiss-Prot;Acc:Q8MIZ1] [ENSMMUT00000029391]	6.99	0.047
granzyme K (granzyme 3; tryptase II) [Source:HGNC Symbol;Acc:4711] [ENSMMUT00000028382]	6.13	0.002
Transferrin Fragment [Source:UniProtKB/TrEMBL;Acc:Q3YAS1] [ENSMMUT00000012466]	6.10	0.015
ST6 (alpha-N-acetyl-neuraminyl-2,3-beta-galactosyl-1,3)-N-acetylgalactosaminide alpha-2,6-sialyltransferase 2 [Source:HGNC Symbol;Acc:10867] [ENSMMUT00000031331]	5.92	0.024
ILLUMIGEN_MCQ_26220 Katze_MMBR Macaca mulatta cDNA clone IBIUW:8552 5' similar to Bases 3 to 1025 highly similar to human TF (Hs.433923), mRNA sequence [CN646444]	5.75	0.041
PREDICTED: Macaca mulatta retinoic acid receptor responder protein 3-like (LOC722189), mRNA [XM_001118373]	4.88	0.021
retinoic acid receptor responder (tazarotene induced) 3 [Source:HGNC Symbol;Acc:9869] [ENSMMUT00000025736]	4.72	0.011
Norrie disease (pseudoglioma) [Source:HGNC Symbol;Acc:7678] [ENSMMUT00000025286]	4.50	0.003
family with sequence similarity 26, member F [Source:HGNC Symbol;Acc:33391] [ENSMMUT00000010359]	4.48	0.012
ring finger protein 183 [Source:HGNC Symbol;Acc:28721] [ENSMMUT00000008196]	4.22	0.041
lipocalin 2 [Source:HGNC Symbol;Acc:6526] [ENSMMUT00000033493]	4.15	0.010
lipocalin 2 [Source:HGNC Symbol;Acc:6526] [ENSMMUT00000033493]	4.12	0.034
PREDICTED: Macaca mulatta tryptophanyl-tRNA synthetase, transcript variant 12 (WARS), mRNA [XM_001105926]	4.03	0.013
PREDICTED: Macaca mulatta ubiquitin [XR_012726]	4.00	0.025
caspase 1, apoptosis-related cysteine peptidase (interleukin 1, beta, convertase) [Source:HGNC Symbol;Acc:1499] [ENSMMUT00000013767]	3.80	0.021
ubiquitin-conjugating enzyme E2L 6 [Source:HGNC Symbol;Acc:12490] [ENSMMUT00000001886]	3.75	0.024
ephrin-A2 [Source:HGNC Symbol;Acc:3222] [ENSMMUT00000031095]	3.70	0.021
fibroblast activation protein, alpha [Source:HGNC Symbol;Acc:3590] [ENSMMUT00000004535]	3.57	0.041
apolipoprotein L, 2 [Source:HGNC Symbol;Acc:619] [ENSMMUT00000002165]	3.50	0.025
Macaca mulatta outer dense fiber of sperm tails 3B (ODF3B), mRNA [NM_001194710]	3.50	0.046
Macaca mulatta CD274 molecule (CD274), mRNA [NM_001083889]	3.41	0.005
sulfatase 1 [Source:HGNC Symbol;Acc:20391] [ENSMMUT00000032745]	3.34	0.040
Macaca mulatta proteasome (prosome, macropain) subunit, beta type, 9 (large multifunctional peptidase 2) (PSMB9), mRNA [NM_001194864]	3.31	0.037
Macaca mulatta integrin beta 1 mRNA, partial cds. [AY878076]	3.23	0.007

PREDICTED: Macaca mulatta protein ALO17-like (LOC718036), mRNA [XM_001110231]	3.19	0.010
Macaca mulatta proteasome (prosome, macropain) subunit, beta type, 9 (large multifunctional peptidase 2) (PSMB9), mRNA [NM_001194864]	3.13	0.029
prostate transmembrane protein, androgen induced 1 [Source:HGNC Symbol;Acc:14107] [ENSMMUT00000031785]	3.09	0.015
signal peptide, CUB domain, EGF-like 3 [Source:HGNC Symbol;Acc:13655] [ENSMMUT00000033135]	3.06	0.041
glutamic pyruvate transaminase (alanine aminotransferase) 2 [Source:HGNC Symbol;Acc:18062] [ENSMMUT00000004645]	2.93	0.026
olfactory receptor, family 51, subfamily E, member 1 [Source:HGNC Symbol;Acc:15194] [ENSMMUT00000020907]	2.79	0.036
Macaca mulatta chemokine (C-C motif) receptor 5 (CCR5), mRNA [NM_001042773]	2.74	0.025
signal transducer and activator of transcription 1, 91kDa [Source:HGNC Symbol;Acc:11362] [ENSMMUT00000007897]	2.73	0.046
ILLUMIGEN_MCQ_28473 Katze_MMPB Macaca mulatta cDNA clone IBIUW:7603 5' similar to Bases 149 to 409 highly similar to human APOL1 (Hs.114309), mRNA sequence [CN647435]	2.67	0.037
baculoviral IAP repeat-containing 3 [Source:HGNC Symbol;Acc:591] [ENSMMUT00000004807]	2.62	0.040
platelet-derived growth factor receptor-like [Source:HGNC Symbol;Acc:8805] [ENSMMUT00000001624]	2.51	0.039
G protein-coupled receptor 115 [Source:HGNC Symbol;Acc:19011] [ENSMMUT00000025228]	2.49	0.006
Sushi-repeat protein [Source:UniProtKB/TrEMBL;Acc:A3FEK9] [ENSMMUT00000011478]	2.48	0.034
F-box protein 6 [Source:HGNC Symbol;Acc:13585] [ENSMMUT00000047575]	2.44	0.016
Macaca mulatta chloride channel accessory 1 (CLCA1), mRNA [NM_001032912]	2.43	0.012
nuclear factor (erythroid-derived 2)-like 3 [Source:HGNC Symbol;Acc:7783] [ENSMMUT00000005121]	2.39	0.008
transmembrane protein 190 [Source:HGNC Symbol;Acc:29632] [ENSMMUT00000022343]	2.36	0.029
Protein HIDE1 Precursor [Source:UniProtKB/Swiss-Prot;Acc:A8MVS5] [ENSMMUT00000026680]	2.36	0.041
F-box protein 6 [Source:HGNC Symbol;Acc:13585] [ENSMMUT00000047575]	2.28	0.032
cell division cycle 25 homolog B (S. pombe) [Source:HGNC Symbol;Acc:1726] [ENSMMUT00000026604]	2.25	0.035
ILLUMIGEN_MCQ_69095 Katze_MMTE Macaca mulatta cDNA clone IBIUW:39364 5' similar to Bases 7 to 610 highly similar to human IFITM3 (Hs.374650), mRNA sequence [DV769955]	2.25	0.036
tumor necrosis factor receptor superfamily, member 9 [Source:HGNC Symbol;Acc:11924] [ENSMMUT00000023238]	2.25	0.046
GRIP and coiled-coil domain containing 2 [Source:HGNC Symbol;Acc:23218] [ENSMMUT00000032158]	2.15	0.045
solute carrier family 6 (neurotransmitter transporter, taurine), member 6 [Source:HGNC Symbol;Acc:11052] [ENSMMUT00000008890]	2.04	0.046
pim-3 oncogene [Source:HGNC Symbol;Acc:19310] [ENSMMUT00000003046]	2.03	0.046
ILLUMIGEN_MCQ_27395 Katze_MMBR Macaca mulatta cDNA clone IBIUW:8115 5' similar to Bases 1 to 600 highly similar to human DSCR6 (Hs.254560), mRNA sequence [CN646916]	1.98	0.047
purinergic receptor P2Y, G-protein coupled, 14 [Source:HGNC Symbol;Acc:16442] [ENSMMUT00000024237]	1.95	0.041
purinergic receptor P2Y, G-protein coupled, 14 [Source:HGNC Symbol;Acc:16442] [ENSMMUT00000024237]	1.93	0.046
ERO1-like (S. cerevisiae) [Source:HGNC Symbol;Acc:13280] [ENSMMUT00000039844]	1.92	0.046
tribbles homolog 3 (Drosophila) [Source:HGNC Symbol;Acc:16228] [ENSMMUT00000017657]	1.69	0.024
PREDICTED: Macaca mulatta mitochondrial inner membrane protease ATP23 homolog (LOC712932), mRNA [XM_001102089]	0.62	0.046
solute carrier family 16, member 10 (aromatic amino acid transporter) [Source:HGNC Symbol;Acc:17027] [ENSMMUT00000030306]	0.55	0.027
Macaca mulatta lymphocyte antigen 6 complex, locus G6C (LY6G6C), mRNA [NM_001194576]	0.55	0.008
acetyl-CoA acyltransferase 1 [Source:HGNC Symbol;Acc:82] [ENSMMUT00000001420]	0.54	0.041
PREDICTED: Macaca mulatta jerky homolog-like (mouse) (JRKL), mRNA [XM_001094262]	0.54	0.041
Macaca mulatta multimerin 2 (MMRN2), mRNA [NM_001193776]	0.53	0.024
membrane-spanning 4-domains, subfamily A, member 13 [Source:HGNC Symbol;Acc:16674] [ENSMMUT00000044282]	0.52	0.010
plexin domain containing 1 [Source:HGNC Symbol;Acc:20945] [ENSMMUT00000006939]	0.49	0.020
matrilin 2 [Source:HGNC Symbol;Acc:6908] [ENSMMUT00000028224]	0.48	0.046
PREDICTED: Macaca mulatta protein kinase, AMP-activated, alpha 2 catalytic subunit (PRKAA2), partial mRNA [XM_002801568]	0.47	0.010
leucine rich repeat transmembrane neuronal 4 [Source:HGNC Symbol;Acc:19411] [ENSMMUT00000043428]	0.46	0.020
ILLUMIGEN_MCQ_10841 Katze_MMPL2 Macaca mulatta cDNA clone IBIUW:9592 5' similar to Bases 1 to 695 highly similar to human PP2135 (Hs.132569), mRNA sequence [CN644776]	0.46	0.041
Macaca mulatta forkhead box C2 (MFH-1, mesenchyme forkhead 1) (FOXC2), mRNA [NM_001198708]	0.46	0.012
PREDICTED: Macaca mulatta keratin-associated protein 13-1-like (LOC712810), mRNA [XM_001101916]	0.45	0.012
klotho [Source:HGNC Symbol;Acc:6344] [ENSMMUT00000023968]	0.45	0.003
Transmembrane protein C20orf123 [Source:UniProtKB/Swiss-Prot;Acc:Q9BR26] [ENSMMUT00000023768]	0.45	0.012
laminin, alpha 3 [Source:HGNC Symbol;Acc:6483] [ENSMMUT00000048264]	0.45	0.041
advillin [Source:HGNC Symbol;Acc:14188] [ENSMMUT00000007486]	0.44	0.033
programmed cell death 4 (neoplastic transformation inhibitor) [Source:HGNC Symbol;Acc:8763] [ENSMMUT00000024185]	0.42	0.025
Macaca mulatta dehydrogenase/reductase (SDR family) member 4 (DHRS4), mRNA [NM_001194475]	0.42	0.049
PREDICTED: Macaca mulatta hypothetical LOC721380 (LOC721380), mRNA [XM_001117508]	0.41	0.041

phosphatidylinositol glycan anchor biosynthesis, class Z [Source:HGNC Symbol;Acc:30596] [ENSMMUT00000045206]	0.41	0.009
calcium/calmodulin-dependent protein kinase II beta [Source:HGNC Symbol;Acc:1461] [ENSMMUT00000003466]	0.39	0.026
protein kinase, AMP-activated, alpha 2 catalytic subunit [Source:HGNC Symbol;Acc:9377] [ENSMMUT00000014567]	0.38	0.021
CNKSR family member 3 [Source:HGNC Symbol;Acc:23034] [ENSMMUT00000002065]	0.38	0.035
PREDICTED: Macaca mulatta insulin-like growth factor binding protein 1, transcript variant 3 (IGFBP1), mRNA [XM_001085935]	0.38	0.027
ILLUMIGEN_MCQ_6817 Katze_MMPL2 Macaca mulatta cDNA clone IBIUW:4419 5' similar to Bases 1 to 1071 highly similar to human FBXO32 (Hs.403933), mRNA sequence [CN802472]	0.37	0.022
PREDICTED: Macaca mulatta 39S ribosomal protein L54, mitochondrial-like (LOC713878), mRNA [XM_001100840]	0.37	0.019
Macaca mulatta KIAA1324-like (KIAA1324L), mRNA [NM_001194030]	0.36	0.006
PREDICTED: Macaca mulatta peroxisomal biogenesis factor 11 alpha, transcript variant 1 (PEX11A), mRNA [XM_001093381]	0.35	0.045
Macaca mulatta dehydrogenase/reductase (SDR family) member 4 (DHRS4), mRNA [NM_001194475]	0.35	0.033
PREDICTED: Macaca mulatta hypothetical protein LOC100424638 (LOC100424638), mRNA [XM_002802655]	0.33	0.035
PREDICTED: Macaca mulatta melanoma associated antigen (mutated) 1-like 1, transcript variant 3 (MUM1L1), mRNA [XM_001092843]	0.31	0.014
BCL2-like 10 (apoptosis facilitator) [Source:HGNC Symbol;Acc:993] [ENSMMUT00000024430]	0.31	0.004
PREDICTED: Macaca mulatta cytochrome c oxidase subunit 6C-like (LOC100423334), mRNA [XM_002802732]	0.30	0.033
protease, serine, 42 [Source:HGNC Symbol;Acc:30716] [ENSMMUT00000020676]	0.30	0.003
PREDICTED: Macaca mulatta ectodysplasin A, transcript variant 1 (EDA), mRNA [XM_001082424]	0.29	0.031
PREDICTED: Macaca mulatta sema domain, immunoglobulin domain (Ig), short basic domain, secreted, (semaphorin) 3B, transcript variant 1 (SEMA3B), mRNA [XM_001102773]	0.28	0.033
HHIP-like 2 [Source:HGNC Symbol;Acc:25842] [ENSMMUT00000011055]	0.27	0.023
phospholipid scramblase 4 [Source:HGNC Symbol;Acc:16497] [ENSMMUT00000045531]	0.27	0.005
leucine rich repeat transmembrane neuronal 4 [Source:HGNC Symbol;Acc:19411] [ENSMMUT00000043428]	0.26	0.002
PREDICTED: Macaca mulatta SH3-domain GRB2-like 2 (SH3GL2), mRNA [XM_001102732]	0.25	0.010
calcium/calmodulin-dependent protein kinase II beta [Source:HGNC Symbol;Acc:1461] [ENSMMUT00000003462]	0.25	0.039
Xg pseudogene, Y-linked 2 [Source:HGNC Symbol;Acc:34022] [ENSMMUT00000048240]	0.25	0.041
Macaca mulatta neuropeptide Y receptor Y5 (NPY5R), mRNA [NM_001032833]	0.25	0.010
PREDICTED: Macaca mulatta hemogen, transcript variant 4 (HEMGN), mRNA [XM_001113799]	0.24	0.041
Uncharacterized protein C1orf115 [Source:UniProtKB/Swiss-Prot;Acc:Q9H7X2] [ENSMMUT00000033027]	0.23	0.008
dynein, axonemal, heavy chain 7 [Source:HGNC Symbol;Acc:18661] [ENSMMUT00000007911]	0.23	0.040
Macaca mulatta neuropeptide Y receptor Y1 (NPY1R), mRNA [NM_001032866]	0.23	0.002
homeobox D1 [Source:HGNC Symbol;Acc:5132] [ENSMMUT00000031334]	0.23	0.024
ATP-binding cassette, sub-family A (ABC1), member 8 [Source:HGNC Symbol;Acc:38] [ENSMMUT00000026133]	0.22	0.012
histidine rich carboxyl terminus 1 [Source:HGNC Symbol;Acc:33872] [ENSMMUT00000022949]	0.22	0.046
Dynein Fragment [Source:UniProtKB/TrEMBL;Acc:Q6UIQ6] [ENSMMUT00000008273]	0.20	0.002
POU class 2 homeobox 3 [Source:HGNC Symbol;Acc:19864] [ENSMMUT00000017160]	0.20	0.008
RUN domain containing 3B [Source:HGNC Symbol;Acc:30286] [ENSMMUT00000009468]	0.20	0.047
protein serine kinase H2 [Source:HGNC Symbol;Acc:18997] [ENSMMUT00000002287]	0.20	0.024
neuropeptide Y receptor Y1 [Source:RefSeq peptide;Acc:NP_001028038] [ENSMMUT00000028477]	0.19	0.002
PREDICTED: Macaca mulatta putative peptide YY-3-like (LOC694766), mRNA [XM_001083655]	0.19	0.024
Macaca mulatta myosin, heavy chain 2, skeletal muscle, adult (MYH2), mRNA [NM_001195292]	0.18	0.041
Macaca mulatta myosin, heavy chain 2, skeletal muscle, adult (MYH2), mRNA [NM_001195292]	0.18	0.010
PREDICTED: Macaca mulatta keratin associated protein 13-2 (KRTAP13-2), mRNA [XM_001099939]	0.17	0.004
metallothionein 1B [Source:HGNC Symbol;Acc:7394] [ENSMMUT00000039322]	0.14	0.037
Dynein Fragment [Source:UniProtKB/TrEMBL;Acc:Q6UIQ6] [ENSMMUT00000008273]	0.14	0.003
retinol binding protein 4, plasma [Source:HGNC Symbol;Acc:9922] [ENSMMUT00000020627]	0.14	0.012
PREDICTED: Macaca mulatta hypothetical LOC701270 (LOC701270), mRNA [XM_001089592]	0.14	0.015
MAM domain containing 2 [Source:HGNC Symbol;Acc:23673] [ENSMMUT00000011666]	0.14	0.002
retinol binding protein 4, plasma [Source:HGNC Symbol;Acc:9922] [ENSMMUT00000020627]	0.14	0.015
SVOP-like [Source:HGNC Symbol;Acc:27034] [ENSMMUT00000030500]	0.12	0.024
metallothionein 1B [Source:HGNC Symbol;Acc:7394] [ENSMMUT00000039324]	0.08	0.006
immunoglobin superfamily, member 21 [Source:HGNC Symbol;Acc:28246] [ENSMMUT00000033081]	0.08	0.046
dehydrogenase/reductase (SDR family) member 7C [Source:HGNC Symbol;Acc:32423] [ENSMMUT00000042221]	0.06	0.002
Uncharacterized protein C11orf16 [Source:UniProtKB/Swiss-Prot;Acc:Q9NQ32] [ENSMMUT00000002826]	0.06	0.010
cytochrome P450, family 3, subfamily A, polypeptide 5 [Source:RefSeq peptide;Acc:NP_001035309] [ENSMMUT00000005022]	0.06	0.015

Table S2

Description	Fold	FDR
acyl-CoA synthetase bubblegum family member 1 [Source:HGNC Symbol;Acc:29567] [ENSMMUT00000016586]	6.00	0.174
interleukin 9 receptor [Source:HGNC Symbol;Acc:6030] [ENSMMUT00000002856]	5.36	0.280
PREDICTED: Macaca mulatta arachidonate 5-lipoxygenase, transcript variant 1 (ALOX5), mRNA [XM_001102354]	5.13	0.174
arachidonate 15-lipoxygenase [Source:HGNC Symbol;Acc:433] [ENSMMUT00000042388]	5.13	0.174
carboxypeptidase A3 (mast cell) [Source:HGNC Symbol;Acc:2298] [ENSMMUT00000007772]	4.85	0.273
membrane-spanning 4-domains, subfamily A, member 2 (Fc fragment of IgE, high affinity I, receptor for; beta polypeptide) [Source:HGNC Symbol;Acc:7316] [ENSMMUT00000018994]	4.71	0.174
arachidonate 5-lipoxygenase [Source:HGNC Symbol;Acc:435] [ENSMMUT00000018848]	4.68	0.202
Putative uncharacterized protein C1orf150 [Source:UniProtKB/Swiss-Prot;Acc:Q5JQS6] [ENSMMUT00000044542]	4.62	0.211
carboxypeptidase A3 (mast cell) [Source:HGNC Symbol;Acc:2298] [ENSMMUT00000007772]	4.49	0.175
PREDICTED: Macaca mulatta mastin-like (LOC722431), mRNA [XM_001118581]	4.46	0.174
tenascin C [Source:HGNC Symbol;Acc:5318] [ENSMMUT00000004742]	4.38	0.174
baculoviral IAP repeat-containing 7 [Source:HGNC Symbol;Acc:13702] [ENSMMUT00000012902]	3.55	0.174
leukotriene C4 synthase [Source:HGNC Symbol;Acc:6719] [ENSMMUT00000017351]	3.53	0.174
acyl-CoA synthetase bubblegum family member 1 [Source:HGNC Symbol;Acc:29567] [ENSMMUT00000016586]	3.45	0.174
tenascin C [Source:HGNC Symbol;Acc:5318] [ENSMMUT00000004742]	3.40	0.288
PREDICTED: Macaca mulatta dermatopontin-like (LOC700181), mRNA [XM_002802062]	3.36	0.273
ghrelin [Source:RefSeq peptide;Acc:NP_001028075] [ENSMMUT00000028003]	3.27	0.213
G protein-coupled receptor 44 [Source:HGNC Symbol;Acc:4502] [ENSMMUT00000000025]	3.14	0.248
Fibronectin 1 Fragment [Source:UniProtKB/TrEMBL;Acc:Q5MD86] [ENSMMUT00000017323]	2.98	0.174
Fibronectin 1 Fragment [Source:UniProtKB/TrEMBL;Acc:Q5MD86] [ENSMMUT00000017323]	2.96	0.174
PREDICTED: Macaca mulatta collagen alpha-1(XIII) chain-like (LOC716986), mRNA [XM_001108092]	2.95	0.175
arachidonate 5-lipoxygenase [Source:HGNC Symbol;Acc:435] [ENSMMUT00000018848]	2.94	0.174
PREDICTED: Macaca mulatta mastin-like (LOC722427), mRNA [XM_001118577]	2.88	0.174
dermatopontin [Source:HGNC Symbol;Acc:3011] [ENSMMUT00000004157]	2.72	0.174
PREDICTED: Macaca mulatta protein FAM38A-like (LOC722206), mRNA [XM_002800862]	2.59	0.174
myosin binding protein H [Source:HGNC Symbol;Acc:7552] [ENSMMUT00000012176]	2.54	0.279
prostaglandin-endoperoxide synthase 1 (prostaglandin G/H synthase and cyclooxygenase) [Source:HGNC Symbol;Acc:9604] [ENSMMUT00000018079]	2.50	0.273
insulin-like growth factor binding protein 6 [Source:HGNC Symbol;Acc:5475] [ENSMMUT00000028608]	2.42	0.174
PREDICTED: Macaca mulatta collagen, type III, alpha 1 (COL3A1), mRNA [XM_001105968]	2.39	0.260
CD320 molecule [Source:HGNC Symbol;Acc:16692] [ENSMMUT00000023457]	2.33	0.246
v-kit Hardy-Zuckerman 4 feline sarcoma viral oncogene homolog [Source:HGNC Symbol;Acc:6342] [ENSMMUT00000004330]	2.17	0.174
ILLUMIGEN_MCQ_32942 Katze_MMBR Macaca mulatta cDNA clone IBIUW:12912 5' similar to Bases 1 to 238 highly similar to human IGFBP6 (Hs.274313), mRNA sequence [CN803406]	2.09	0.175
PREDICTED: Macaca mulatta cysteine-rich secretory protein LCCL domain containing 2, transcript variant 3 (CRISPLD2), mRNA [XM_001112988]	2.02	0.193
PREDICTED: Macaca mulatta prostaglandin-endoperoxide synthase 1, transcript variant 6 (PTGS1), mRNA [XM_001088270]	2.01	0.280
Macaca mulatta collagen type III alpha 1 mRNA, 3' UTR. [FJ932748]	1.98	0.273
spondin 1, extracellular matrix protein [Source:HGNC Symbol;Acc:11252] [ENSMMUT00000030829]	1.83	0.288
early B-cell factor 4 [Source:HGNC Symbol;Acc:29278] [ENSMMUT00000044592]	1.82	0.174
ArfGAP with GTPase domain, ankyrin repeat and PH domain 1 [Source:HGNC Symbol;Acc:16922] [ENSMMUT00000013063]	1.80	0.174
zinc finger protein 620 [Source:HGNC Symbol;Acc:28742] [ENSMMUT00000022433]	1.76	0.279
Macaca mulatta carbonyl reductase 3 (CBR3), mRNA [NM_001193746]	1.68	0.267
insulin-like growth factor 1 receptor [Source:HGNC Symbol;Acc:5465] [ENSMMUT00000017236]	1.43	0.282
F-box protein 6 [Source:HGNC Symbol;Acc:13585] [ENSMMUT00000047575]	0.65	0.273
Macaca mulatta haloacid dehalogenase-like hydrolase domain containing 3 (HDHD3), mRNA [NM_001194198]	0.56	0.271
signal transducer and activator of transcription 1, 91kDa [Source:HGNC Symbol;Acc:11362] [ENSMMUT00000007897]	0.51	0.174
ubiquitin-conjugating enzyme E2L 6 [Source:HGNC Symbol;Acc:12490] [ENSMMUT00000001886]	0.49	0.174
CD5 molecule-like [Source:HGNC Symbol;Acc:1690] [ENSMMUT00000027876]	0.48	0.287
PREDICTED: Macaca mulatta ubiquitin [XR_012726]	0.47	0.175
retinoic acid receptor responder (tazarotene induced) 3 [Source:HGNC Symbol;Acc:9869] [ENSMMUT00000025736]	0.45	0.280
PREDICTED: Macaca mulatta thymidine phosphorylase, transcript variant 4 (TYMP), mRNA [XM_001112945]	0.45	0.288
G protein-coupled receptor 128 [Source:HGNC Symbol;Acc:19241] [ENSMMUT00000004053]	0.43	0.174
PREDICTED: Macaca mulatta retinoic acid receptor responder protein 3-like (LOC722189), mRNA [XM_001118373]	0.41	0.174
PREDICTED: Macaca mulatta hypothetical LOC703547, transcript variant 1 (LOC703547), mRNA [XM_001099113]	0.40	0.288
PREDICTED: Macaca mulatta hypothetical LOC703547, transcript variant 1 (LOC703547), mRNA [XM_001099113]	0.40	0.288
PREDICTED: Macaca mulatta guanylate-binding protein 6-like (LOC695158), miscRNA [XR_091839]	0.39	0.174
CD8a molecule [Source:HGNC Symbol;Acc:1706] [ENSMMUT00000004986]	0.39	0.288
Macaca mulatta indoleamine 2,3-dioxygenase 1 (IDO1), mRNA [NM_001077483]	0.39	0.174
Macaca mulatta indoleamine 2,3-dioxygenase 1 (IDO1), mRNA [NM_001077483]	0.38	0.273
tubulointerstitial nephritis antigen [Source:HGNC Symbol;Acc:14599] [ENSMMUT00000017935]	0.32	0.174
sciellin [Source:HGNC Symbol;Acc:10573] [ENSMMUT00000000066]	0.30	0.282
PREDICTED: Macaca mulatta thymidine phosphorylase, transcript variant 4 (TYMP), mRNA [XM_001112945]	0.29	0.288
ring finger protein 182 [Source:HGNC Symbol;Acc:28522] [ENSMMUT00000041378]	0.27	0.202
C-X-C motif chemokine 10 Precursor (Small-inducible cytokine B10)(10 kDa interferon-gamma-induced protein)(Gamma-IP10)(IP-10) [Source:UniProtKB/Swiss-Prot;Acc:Q8MIZ1] [ENSMMUT00000029391]	0.27	0.174
Macaca mulatta chemokine (C-X-C motif) ligand 10 (CXCL10), mRNA [NM_001032892]	0.24	0.174
tumor protein p63 regulated 1 [Source:HGNC Symbol;Acc:24759] [ENSMMUT00000009593]	0.23	0.174
PREDICTED: Macaca mulatta hephaestin-like 1 (HEPHL1), mRNA [XM_001086917]	0.22	0.175
Macaca mulatta chemokine (C-X-C motif) ligand 11 (CXCL11), mRNA [NM_001032950]	0.19	0.174
small inducible cytokine B11 [Source:RefSeq peptide;Acc:NP_001028122] [ENSMMUT00000029393]	0.16	0.174

Table S3

ProbeID	Description	Fold	FDR
A_01_P1692126		38.239	0.04064
A_01_P1819261		37.096	0.00087
A_01_P1703526		18.885	0.00781
A_01_P1802881		11.94	0.04064
A_01_P1832812		10.216	0.01363
A_01_P1793846		6.044	0.01301
A_01_P006328	sphingosine-1-phosphate phosphatase 2 [Source:HGNC Symbol;Acc:19953] [ENSMMUT00000010762]	4.448	0.02617
A_01_P012199	paraoxonase 3 [Source:HGNC Symbol;Acc:9206] [ENSMMUT00000011208]	0.068	0.04831
A_01_P1825581	PREDICTED: Macaca mulatta 40S ribosomal protein S27-like (LOC696068), mRNA [XM_001084710]	0.061	0.00242
A_01_P020134	PREDICTED: Macaca mulatta mediator complex subunit 17, transcript variant 4 (MED17), mRNA [XM_001088365]	0.05	0.00474
A_01_P1696961	Macaca mulatta clone 464LK1 immunoglobulin kappa light chain (IGK) mRNA, partial cds. [FJ795842]	0.018	0.00711
A_01_P1736386		0.016	0.00058
A_01_P1736376		0.014	0.01937
A_01_P1694966	immunoglobulin kappa constant [Source:HGNC Symbol;Acc:5716] [ENSMMUT00000029842]	0.012	0.00058
A_01_P1682792	immunoglobulin kappa constant [Source:HGNC Symbol;Acc:5716] [ENSMMUT00000029842]	0.011	0.00058
A_01_P1736936		0.011	0.01039
A_01_P1697811	Macaca mulatta Ig rearranged light chain variable region, anti-RBC antibody, mRNA, partial cds. [U57571]	0.011	0.00347
A_01_P1699936		0.01	0.01247
A_01_P1696840	immunoglobulin kappa constant [Source:HGNC Symbol;Acc:5716] [ENSMMUT00000029842]	0.009	0.00079
A_01_P1736906	PREDICTED: Macaca mulatta hypothetical LOC707609 (LOC707609), mRNA [XM_001096027]	0.008	0.04064
A_01_P1697816	Macaca mulatta Ig rearranged light chain variable region, anti-RBC antibody, mRNA, partial cds. [U57572]	0.008	0.00908
A_01_P1696981	Macaca mulatta clone 464LK8 immunoglobulin kappa light chain (IGK) mRNA, partial cds. [FJ795847]	0.007	0.0193
A_01_P1696176	immunoglobulin kappa constant [Source:HGNC Symbol;Acc:5716] [ENSMMUT00000029842]	0.007	0.00058
A_01_P1736381	immunoglobulin kappa constant [Source:HGNC Symbol;Acc:5716] [ENSMMUT00000029842]	0.007	0.00058
A_01_P1696856	immunoglobulin kappa constant [Source:HGNC Symbol;Acc:5716] [ENSMMUT00000029842]	0.007	0.00087
A_01_P1682796	Macaca mulatta Ig rearranged light chain variable region, anti-RBC antibody, mRNA, partial cds. [U57570]	0.006	0.00079
A_01_P1696181	Macaca mulatta clone D0(8) immunoglobulin light chain mRNA, partial cds. [AY994523]	0.006	0.00058

A_01_P1698851	Macaca mulatta clone D0(2) immunoglobulin light chain mRNA, partial cds. [AY994517]	0.006	0.00058
A_01_P1682936	Macaca mulatta Ig rearranged light chain variable region, anti-RBC antibody, mRNA, partial cds. [U57575]	0.006	0.01238
A_01_P1701676	Macaca mulatta clone S19 immunoglobulin kappa light chain mRNA, partial cds. [AY452636]	0.006	0.00058
A_01_P1701661	Macaca mulatta Ig rearranged light chain variable region, anti-RBC antibody, mRNA, partial cds. [U57570]	0.006	0.00064
A_01_P1736396		0.006	0.02009
A_01_P1696186	Macaca mulatta clone D0(15) immunoglobulin light chain mRNA, partial cds. [AY994524]	0.006	0.00058
A_01_P1701671		0.006	0.00434
A_01_P1736921		0.006	0.00938
A_01_P1697821	Macaca mulatta Ig rearranged light chain variable region, anti-RBC antibody, mRNA, partial cds. [U57574]	0.005	0.00288
A_01_P1696196	Macaca mulatta clone D21(15) immunoglobulin light chain mRNA, partial cds. [AY994526]	0.005	0.00058
A_01_P1736366	PREDICTED: Macaca mulatta hypothetical protein LOC100424267 (LOC100424267), mRNA [XM_002799331]	0.005	0.00087
A_01_P1736391		0.005	0.00079
A_01_P1736896		0.005	0.01301
A_01_P1682931	Macaca mulatta Ig rearranged light chain variable region, anti-RBC antibody, mRNA, partial cds. [U57579]	0.005	0.00058
A_01_P1818496		0.005	0.01301
A_01_P1672341		0.005	0.0012
A_01_P1695881	Macaca mulatta clone 4S7K2_S22 immunoglobulin kappa chain (IgK) mRNA, partial cds. [AY452596]	0.004	0.03106
A_01_P1682926	Macaca mulatta clone B417K immunoglobulin kappa light chain (IGK) mRNA, partial cds. [HM044989]	0.004	0.02009
A_01_P1736881	Macaca mulatta clone B442K immunoglobulin kappa light chain (IGK) mRNA, partial cds. [HM044994]	0.004	0.01258
A_01_P1736916	Macaca mulatta clone B408K immunoglobulin kappa light chain (IGK) mRNA, partial cds. [HM044987]	0.004	0.02142